Combustion Theory and Modelling
Vol. 00, No. 00, July 2013, 1–35

Published in Combust. Theory and Modelling, (2014), 18(2), p.295-329
DOI: 10.1080/13647830.2014.898409

RESEARCH ARTICLE

Modelling of Turbulent Lifted Jet Flames using flamelets: *a priori* assessment and *a posteriori* validation

S. Ruan*, N. Swaminathan**, O. Darbyshire+

Department of Engineering, Cambridge University, Cambridge CB2 1PZ, UK

(*First submitted 11 July 2013. Revised 3 February 2014. Accepted 15 February 2014.*)

This study focuses on the modelling of turbulent lifted jet flames using flamelets and presumed PDF approach with interests on both flame lift-off height and flame brush structure. First, flamelet models used to capture contributions from premixed and non-premixed modes to the partially premixed combustion in the lifted jet flame are assessed using a Direct Numerical Simulation (DNS) data for turbulent lifted hydrogen jet flame. The joint PDFs of mixture fraction, Z, and progress variable, c, including their statistical correlation are obtained using a copula method, which is also validated using the DNS data. The statistically independent PDFs are found to be generally inadequate to represent the joint PDFs from the DNS data. The effects of Z-c correlation and contribution from non-premixed combustion mode on the flame lift-off height are studied systematically by including one effect at a time in the simulations used for *a posteriori* validation. A simple model including the effects of chemical kinetics and scalar dissipation rate is suggested and used for non-premixed combustion contributions. The results clearly show that both Z-c correlation and non-premixed combustion effects are required in the premixed flamelets approach to get a good agreement with the measured flame lift-off heights as function of jet velocity. The flame brush structure reported in earlier experimental studies is also captured reasonably well for various axial positions. It seems that the flame stabilisation is influenced by both premixed and non-premixed combustion modes, and their mutual influences.

Keywords: Turbulent jet lifted flame; Presumed joint PDF with correlation; Mean reaction rate closure; Flame lift-off height; Lifted flame stabilisation

1. Introduction

Turbulent lifted flames established downstream of a fuel jet have been the subject of many past studies because the configuration is relatively simple and yet practically relevant. The stabilisation of these flames is a manifestation of complex interplay between many physical processes [1–3] such as partial premixing of fuel resulting from entrainment of surrounding air, flame propagation [4], interaction between flame leading edge and large-scale flow structure [5–7], edge-flame propagation [8], triple-flames [9–12] and possibly extinction of non-premixed flamelets due to high scalar dissipation rate near the leading edge [13]. In the presence of a heated co-flow with sufficiently high temperature, autoignition [7, 14–16] plays an important role as well. This richness in physics offers considerable challenge to model these lifted flames. Turbulent lifted jet flames without co-flow have been modelled in the past using various methodologies, such as the G-equation or level-set approach [17–19], the flamelets model involving premixed and non-premixed flamelets [20–27] and Conditional Moment Closure (CMC) [28–30]. In the presence of a heated co-flow, the transported PDF method [31] has been also used.

* Corresponding author. Email: sr468@cam.ac.uk
**Email: ns341@cam.ac.uk
+ Present Address: BAE Systems Advanced Technology Centre, Sowerby Building (20R), Golf Course Lane, Filton, Bristol BS34 7QW

ISSN: 1364-7830 print/ISSN 1741-3559 online

DOI: 10.1080/13647830.YYYY.xxxxxx
http://www.tandfonline.com

Among these approaches, the flamelet model with tabulated chemistry [27, 32, 33] is relatively simple and computationally less expensive either for LES (large eddy simulation) or RANS (Reynolds averaged Navier-Stokes) methodologies. Domingo et al. [14, 22] combined premixed and non-premixed flamelets to model the filtered reaction rate required in LES after determining the local burning mode using a transport equation for a flame index introduced by Yamashita et al. [34]. A flamelet transformation was employed in [35] to distinguish the local burning mode in a LES calculation. In these approaches, the filtered reaction rate was computed as a sum of premixed and non-premixed contributions weighted by the burning mode indicator. This required an extra transport equation for the burning mode to be carried in the simulation and further modelling for its unclosed terms. This method has been used to calculate lifted flames of hydrogen [22] and methane [25] using LES.

Bradley and his co-workers [20, 21, 36] used a range of premixed flamelets spanning the flammability limit to model the lifted jet flame using RANS methodology. The turbulence stretch effects were included using a burning rate factor, an empirical relation involving the Karlovitz and Markstein numbers, in their approach. In the above flamelet approach for RANS and LES of partially premixed combustion, one gets the required mean or filtered reaction rate using

$$\overline{\dot{\omega}} = \int_0^1 \int_0^1 \dot{\omega}(\zeta, \xi) \;\; P(\zeta, \xi) \quad d\zeta \; d\xi, \tag{1}$$

where ξ and ζ are sample space variables for the mixture fraction, Z, and reaction progress variable, c. The symbol $\dot{\omega}(\zeta, \xi)$ denotes the flamelets reaction rate when the flamelets chemistry can be described using the two variables ζ and ξ. The joint PDF, $P(\zeta, \xi)$ was invariably obtained in past studies using presumed shapes for the marginal PDFs after assuming the statistical dependence of Z and c to be weak. A Beta function for ξ and a double delta function for ζ were the common choices. The assumption of statistical independence is not always justified, especially near the flame base in a lifted jet flame [37]. Experimental [9, 11, 12] and DNS [10, 38] studies showed the presence of premixed and non-premixed flames as triple flames influencing one another near the leading edge of the lifted flames. The presence of triple flames at the base of a lifted flame has been recognised in many earlier studies. Thus, the validity of the statistical independence of Z and c near the leading edge is questionable. So, alternative methods need to be found to avoid the assumption of statistical independence.

Darbyshire [39] and Darbyshire and Swaminathan [40] have developed a method to eliminate this assumption by using a *copula* to build the joint PDF of Z and c from their marginal PDFs according to a prescribed correlation. This approach was tested for turbulent stratified V flames with stratification on the lean side of the stoichiometry and the results were encouraging [39, 40]. The performance of this approach for partially premixed combustion covering the whole range of stoichiometry has yet to be tested. The turbulent lifted flame, especially the flame base, is an ideal candidate for this test. Thus, the main objective of this study is to simulate turbulent lifted jet flames established by a hydrogen jet into a quiescent air using the flamelets, reviewed in section 2, for thermochemistry and *copula*, discussed in section 3.3, for the joint PDF. Here, RANS methodology is followed because of its low computational expenses and to assess the ability of this modelling approach before attempting LES in a future work.

The specific aim of this study is twofold. Firstly, *a priori* assessment of combustion modelling with both premixed and non-premixed flamelets, and presumed PDFs using DNS data of a lifted hydrogen jet flame [10, 38] is conducted. It is of interest to test whether the use of unstrained premixed and strained non-premixed flamelets make any difference for the mean reaction rate since some studies [26] showed that these two

flamelets are equally good, despite the difference in the physics of these two flamelets. Previous studies using DNS [41] and RANS [42, 43] showed that strained premixed flamelets established in opposed flow of reactant and product may be more appropriate than the unstrained flamelets for turbulent premixed combustion. Thus, it is of interest here to examine whether the strained flamelets can be used to model lifted flames. Also, the effects of including the statistical correlation in the joint PDF required for the mean reaction rate closure are investigated.

Secondly, *posteriori* validation is performed by computing turbulent lifted hydrogen jet flames for a range of jet velocities using the combustion models explored in the first part on *a priori* testing. This would help us to elucidate the roles and contributions of premixed and non-premixed combustion modes, and the statistical correlation of Z and c.

This paper is organised as follows. The flamelets modelling framework of partially premixed combustion used in this study is reviewed briefly in section 2. *A priori* assessments to fulfil the first aim of this study are discussed in section 3 after introducing the DNS data and its processing techniques. A detailed description of the *copula* method is provided in subsection 3.3 along with its *a priori* assessment. Various flamelets closures explored in this study are discussed in subsection 3.4. The roles of scalar dissipation rates identified in section 2 are discussed in subsection 3.5 along with simple models for them. The detail of the test case, its computational models and boundary conditions used for *posteriori* validation along with the computational results and their comparison to measurements are discussed in section 4. The conclusions of this study are summarised in the final section.

2. Partially premixed combustion modelling

An exact transport equation for instantaneous reaction progress variable c can be written as [14, 15, 22, 44]

$$\frac{\partial \rho c}{\partial t} + \frac{\partial \rho u_j c}{\partial x_j} = \frac{\partial}{\partial x_j}\left(\rho D \frac{\partial c}{\partial x_j}\right) + \dot{\omega}_c^*. \tag{2}$$

for partially premixed combustion. The source term $\dot{\omega}_c^*$ is given by

$$\dot{\omega}_c^* = \frac{1}{\partial Y_i/\partial c}\left(\dot{\omega}_i + 2\rho N_{cZ}\frac{\partial^2 Y_i}{\partial c \partial Z} + \rho N_{zz}\frac{\partial^2 Y_i}{\partial Z^2} + \rho N_{cc}\frac{\partial^2 Y_i}{\partial c^2}\right), \tag{3}$$

if c is defined using mass fraction of scalar i. The above equation contains contribution from chemical reactions involving species i and the three dissipation rates arising due to the dependence of c on Z. These dissipation rates are defined as

$$N_{zz} = \rho D(\nabla Z \cdot \nabla Z), \quad N_{cz} = \rho D(\nabla c \cdot \nabla Z) \text{ and } N_{cc} = \rho D(\nabla c \cdot \nabla c), \tag{4}$$

where D is the molecular diffusivity which is taken to be equal for the progress variable and mixture fraction for simplicity. Equation (3) is strictly valid when the molecular diffusivities of all species are equal. This would imply that $D_Z = D_c = D$. Allowing the molecular diffusivities to be different for different species would introduce additional terms in Eq. (3) because of differential diffusion effect, which may be negligible for high Reynolds number flows as noted by Ruan et al. [37].

In the limit of purely premixed combustion, the terms involving the scalar dissipation rates in Eq. (3) are zero. In the limit of non-premixed combustion, it was shown [15, 22] that this equation reduces to the well-known steady diffusion flamelet equation.

The lifted flame is usually considered as a non-premixed flame and thus, the mean

reaction rate can be obtained as [19, 45, 46]

$$\bar{\dot{\omega}}_i = \int\int \dot{\omega}_i(\xi,\chi)\ P(\xi,\chi) \quad d\xi\ d\chi, \tag{5}$$

using non-premixed flamelets. The symbols ξ and χ are the sample space variable for the mixture fraction Z and the scalar dissipation rate of mixture fraction N_{zz} respectively. However, experimental [9, 11, 12] and DNS [10, 38] studies showed the presence of triple flames at the base of the lifted flames and both premixed and diffusion combustion in the downstream positions and hence one must use the full form of Eq. (3) and include *Z-c* correlation to calculate the mean reaction rate in partially premixed combustion. This approach is followed in this study and its *a priori* assessment is discussed in the next section.

3. *A priori* assessment using DNS data

DNS data of a turbulent lifted hydrogen jet flame is used for *a priori* assessment of flamelets/presumed PDF models based on Eq. (3). The DNS data and its processing techniques are discussed first briefly. This is followed by a detailed examination of the joint PDF, $P(\xi,\zeta)$, in Eq. (1) and its modelling. The mean reaction rate closure given by Eq. (1) is explored using various combination of premixed and non-premixed flamelets and then the contribution from the term involving dissipation rates in Eq.(3) is discussed.

3.1 DNS data

A detailed discussion on the DNS data used in this study is given in references [10] and [38]. Thus, only a brief discussion identifying the salient features relevant for the current investigation is given here. A turbulent lifted flame established by a hydrogen jet issuing from a round nozzle into quiescent air was simulated using DNS methodology by Mizobuchi et al. [10, 38]. The jet Mach number is 0.54 and the Reynolds number based on the nozzle diameter, D = 2 mm, and bulk mean velocity of 680 m/s is 13,600. Figure 1 shows a schematic of this configuration along with time averaged temperature field and stoichiometric mixture fraction contour. Four cross sections labelled A, B, B1 and C in this figure, located at x/D = 5.75, 8.75, 11.75 and 14.75 respectively, are used for later investigation. The streamwise, y, and radial, R, distances are normalized using D. The size of the computational domain is $\pm 12.5D$ in cross-stream and $-2D$ to $20D$ in streamwise directions respectively. This domain is discretised using a non-uniform grid with a total of about 200 millions grid points with a uniform grid spacing of 0.05 mm for $\pm 5D \times 14.75D \times \pm 5D$ region. This grid spacing is about 2.5 times the Kolmogorov scale close to ignition point in the experiment [47, 48]. The ratio between the stoichiometric laminar premixed flame thermal thickness and the mesh resolution is 10. This resolution was shown to be sufficient to gather scalar gradient related statistics in earlier studies [10, 37, 38] and thus the DNS is considered to be well-resolved for the purpose of this investigation. This DNS used detailed transport properties and a chemical kinetics mechanism, involving 9 species (including nitrogen as an inert species) and 17 reactions [49]. The lifted flame is stabilised at about $5.5D$ from the nozzle exit. This lifted hydrogen jet flame has been investigated experimentally in references [47] and [48] and this experimental data is used for *posteriori* validation in section 4.

3.2 Data Processing

The data processing technique is detailed by Ruan et al. [37] and a brief summary is given here. The statistics at a given cross section are constructed by splitting the cross section into a number of concentric rings. The radial distance R is measured from the jet centre ($R = 0$). All the sample points in a particular ring of width dr are averaged to obtain a mean value, calculated as

$$\bar{Q}(R, y) = \frac{1}{N_t} \sum_{t_i=1}^{N_t} \frac{1}{N} \sum^{N} Q(x, z, t_i;\ y), \tag{6}$$

where Q is the quantity of interest, N_t is the number of samples over a time period of 0.08 ms, about twice the flow through time, and N is the total number of data points in a particular ring of width dr for a single time sampling. The time and spatial, in homogeneous direction, averaging are combined to increase the sample size since the flow and flame have reached statistically stationary state [37]. Various ring widths of $2\,dh$ and $4\,dh$, where dh is the mesh spacing in the cartesian system used for the DNS, had been tested and gave similar results [37]. Statistical convergence for the results presented here has also been verified by more than doubling the the sample size and sampling duration. The scalar gradients required in the analysis are calculated using a central differencing scheme.

The mixture fraction is calculated using [50]

$$Z = \frac{Z_{\mathrm{H}}/W_{\mathrm{H_2}} + 2(Y_{\mathrm{O_2,air}} - Z_{\mathrm{O}})/W_{\mathrm{O_2}}}{1/W_{\mathrm{H_2}} + 2Y_{\mathrm{O_2,air}}/W_{\mathrm{O_2}}}, \tag{7}$$

where Z_i is the mass fraction of element i, $W_{\mathrm{O_2}} = 32$, $W_{\mathrm{H_2}} = 2$, and $Y_{\mathrm{O_2,air}} = 0.244$ is the mass fraction of O_2 in air, with 22% O_2 and 78% N_2 by volume. The stoichiometric mixture fraction Z_{st} is about 0.03. The mixture fraction diffusivity D_Z is calculated with a mass weighted individual species diffusivity D_i as $D_Z = \sum Y_i D_i$. It is to be noted that $D_Z \approx D_{\mathrm{N2}}$ because of the dominance of nitrogen, which has a Lewis number close to unity.

The progress variable, c, is defined in this paper using $Y_{\mathrm{H_2O}}$ as

$$c(Z) = \frac{Y_{\mathrm{H_2O}}(Z)}{Y^{Eq}_{H_2O}(Z)}, \tag{8}$$

where $Y^{Eq}_{H_2O}(Z)$ is the equilibrium value of H_2O mass fraction at the mixture fraction value of Z. The molecular diffusivity of this c is $D_{\mathrm{H_2O}}$ and the Lewis number for H_2O is close to unity.

3.3 Validation of presumed joint PDFs

Before examining the joint PDF of Z and c, their marginals PDFs are to be examined. Figure 2 shows these marginal PDFs extracted from the DNS data at several representative radial and axial positions of interest. The location for $P(\zeta)$ is chosen so that there is a non-trivial variation of this PDF and substantial mean reaction rate. This can be seen by verifying these locations approximately in Fig.1. For $P(\xi)$, these locations vary from the jet centre to the middle of the flame brush. This helps us to see the general variation of the mixture fraction PDF at these typical locations. The β function PDF commonly used for these scalars [46, 51] is also shown. The agreement is seen to be reasonably good for both Z and c. The progress variable PDF is observed to be bimodal in the upstream position (A-A, $R/D = 2.5$) with non-negligible burning part. This PDF is monomodal for

downstream positions where the local mixture is predominantly unburnt or burnt gases. These bimodal and monomodal shapes are represented reasonably well by the β function PDF and the agreement is very good for the mixture fraction PDF. Thus, these marginal PDFs are used to construct the correlated joint PDF, $P(\xi, \zeta)$, using a *copula* for a given value of covariance $\widetilde{c''Z''}$.

A *copula* can be understood as a functional that couples multivariate distributions to their marginal distributions. The general procedure involved in this approach is briefly summarised below [39, 40]. The details of this approach are given in [40].

(1) A correlation coefficient is calculated from given values of covariance of ξ and ζ, and their respective standard deviations, σ_ξ and σ_ζ, using

$$r_{\xi\zeta} = \frac{\mathrm{Covar}(\xi, \zeta)}{\sigma_\xi \sigma_\zeta}. \tag{9}$$

(2) Two large, say 5,000, sets of independent random numbers, η_i and ψ_i are generated using standard normal distributions. The subscript i runs from 1 to 5,000.

(3) The correlation coefficient $r_{\eta\psi}$ of the random variables η_i and ψ_i is related to the desired correlation $r_{\xi\zeta}$ through

$$r_{\eta\psi} = 2 \sin\left(\frac{\pi\, r_{\xi\zeta}}{6}\right). \tag{10}$$

(4) A new set of random variables $(\eta_i, \psi_i^{\mathrm{new}})$, having the required correlation $r_{\eta\psi}$ are calculated using

$$\psi_i^{\mathrm{new}} = \eta_i\, r_{\eta\psi} + \psi_i \sqrt{1 - r_{\eta\psi}^2}. \tag{11}$$

(5) The random variables η_i and ψ_i^{new} are transformed to a uniform distribution by using the cumulative distribution function (CDF), Φ, for the standard normal distribution

$$\xi_i = \Phi(\eta_i) = \frac{1}{2}\left[1 + \mathrm{erf}\left(\frac{\eta_i}{\sqrt{2}}\right)\right] \quad \text{and} \quad \zeta_i = \Phi(\psi_i^{\mathrm{new}}), \tag{12}$$

where erf is the error function.

(6) The Plackett coupla [52] is chosen here because of its simplicity. The odds ratio, θ, required for constructing the joint PDF through this copula [52] is calculated by plotting the uniformly distributed ξ_i and ζ_i in the contingency table, illustrated in Fig. 3. Then, one counts the number of samples, N_i, falling in each of the four quadrants shown in that figure. The number of samples falling in the range $0 \le \xi < 0.5$ and $0 \le \zeta < 0.5$ is N_1 and the number of samples in the range $0.5 \le \xi \le 1.0$ and $0.5 \le \zeta \le 1.0$ is N_3. A similar counting is used for N_2 and N_4 noted in Fig. 3. The odds ratio, θ, is then obtained as

$$\theta = \frac{N_1 N_4}{N_2 N_3}. \tag{13}$$

(7) Finally, the joint PDF with a desired correlation coefficient, $r_{\xi\zeta}$, is calculated as

$$p(\xi, \zeta) = \begin{cases} \dfrac{\theta f g \{1 + (\theta - 1)[F + G - 2FG]\}}{[S^2 - 4\theta(\theta - 1)FG]^{3/2}} & \text{if } \theta \neq 1 \\ f g & \text{if } \theta = 1 \end{cases} \tag{14}$$

where $S = 1 + (\theta - 1)(F + G)$, and f and g are the marginal PDFS from the beta function for ξ and ζ respectively. F and G are their respective CDFs. The case $\theta = 1$ is the statistically independent case.

It is worth noting that the size of random number sample used in the step (2) above should be as large as possible to ensure the statistical convergence of $\overline{\dot{\omega}}$. A test is conducted using the sample size ranging from 80 to 10^5. Since $\dot{\omega}(\zeta, \xi)$ in Eq. (1) is kept the same for this test, the influence of the sample size comes through the joint pdf $P(\zeta, \xi)$. The result of this test is shown in Fig. 4, where the error in the mean reaction rate with respect to the value obtained for the case with 10^5 samples is shown as a function of the sample size. This result is shown for the stoichiometric mixture with arbitrarily chosen values for other parameters given in Fig. 4. The error is less than 1% for the case with 5000 samples for various covariance values shown in this figure and thus this sample size is used in this study. A similar behaviour is observed for other equivalence ratios.

Figure 5 shows typical joint PDFs obtained from the DNS data for several radial and axial positions along with the modelled PDFs for the corresponding locations. The statistically independent and correlated models are considered. The means, variances and covariances required for the models are extracted from the DNS data appropriately. The positions shown in Fig. 5 are chosen to be representative of various conditions that can exists in partially premixed combustion. At the radial position of $R/D = 2.0$ at A-A, the mean temperature is high as shown in Fig. 1. This location is close to the flame stabilisation region. The joint PDF from the DNS data indicates that there is substantial unreacted mixture, i.e. $\zeta \approx 0$, spanning a wide range of mixture fraction and has a long tail extending to rich mixture up to $\xi = 0.4$. This long tail is not shown in this figure. There is also a substantial pocket of hot product of stoichiometric and lean mixtures with $\zeta > 0.8$. The representation of this joint PDF by both models is reasonable for this position, which is consistent with previous study [37] showing that Z-c correlation at upstream position is small. However, the correlated joint PDF gives slightly improved results in terms of location for the peak PDF value near $\zeta \approx 1$and the width of this PDF value in the mixture fraction, $0 < \xi < 0.02$, space. A substantial improvement is not expected for this location since the covariance value is small as shown in [37]. The second row of Fig. 5 presents the joint PDF at a downstream position B-B and $R/D = 1$, which is in the middle of the flame-brush having $\bar{c} \approx 0.5$. The burning mixture at this location is substantially rich and a negative correlation can also be seen. The correlated PDF obtained using the *copula* captures this correlation and agrees well with the DNS results compared to the uncorrelated model. Similar behaviour is observed for another downstream position, C-C and $R/D = 1$, shown in the third row of Fig. 5. The results shown in the bottom row of Fig. 5 is for the position C-C and $R/D = 2.5$, which is close to the burnt side with $\zeta \approx 1$. Although there is still substantial burning, signified by the PDF magnitude for $0.2 \leq \zeta \leq 0.8$, a negative correlation can be seen and there is a significant probability to find equilibrium products, $\zeta \approx 1$, of rich mixture. These attributes are represented well by the correlated PDF compared to the statistically independent PDF model as one observes in Fig. 5. It is also worth to note that the use of coupla does not dependent on definition of c and it has been used in earlier studies [39, 40] for c based on carbon dioxide mass fraction and for a different flame configuration.

3.4 Mean reaction rate closure

The progress variable source term, $\dot{\omega}_c^*$, for partially premixed combustion has four components as noted in Eq. (3) and the focus for this section is on the first term $\overline{\dot{\omega}_c}$ and its possible closure. The other terms involving the scalar dissipation rates will be dealt in the next section.

Four different modelling methods summarised in Table 1 are considered in this study.

One common approach is to use Eq. (1) to tabulate the mean reaction rate as a function of means, variances and covariance. The phase-space relation, $\dot{\omega}(\zeta, \xi)$, in Eq. (1) is obtained using unstrained premixed flamelets for a range of mixture fraction values. This approach is also known as Flamelet Generated Manifold (FGM) [32] or the Flame Prolongation ILDM (FPI) [33], where the joint PDF is taken to be a product of two presumed marginal PDFs, ie., $P(\zeta, \xi) = P_\beta(\zeta)P_\beta(\xi)$. This is the first model for the mean reaction rate, called **M1** in this study. For the second model, **M2**, the correlated joint PDF obtained by the method described in section 3.3 is used in Eq. (1). The non-premixed flamelet model in Eq.(5) is used along with a β function PDF for Z and a log-normal PDF [53, 54] for χ. This model is referred as **M3** in Table 1 and the joint PDF is calculated as $P(\xi, \chi) = P_\beta(\xi)P_{\log N}(\chi)$ since the statistical independence of Z and χ is known to hold when $P(\xi)$ is monomodal with its peak in $0 < \xi < 1$ [55]. The fourth model, **M4**, considers the strained premixed flamelets along with the presumed PDFs listed in Table 1. Since the strained premixed flamelets were shown to work well for turbulent premixed jet flames [42, 43], it is of interest to test if a direct extension of the strained flamelets formulation to partially premixed combustion can be made. The mean reaction rate is calculated as

$$\overline{\dot{\omega}}_c = \int\int\int \dot{\omega}_c(\zeta, \xi, \psi)\, P(\zeta, \xi, \psi)\;\; d\zeta\, d\xi\, d\psi, \tag{15}$$

where ψ is the sample space variable for the scalar dissipation N_{cc}. The trivariate PDF is obtained using $P(\zeta, \xi, \psi) = P(\psi|\zeta)P(\zeta)P(\xi)$ and $P(\psi|\zeta)$ is presumed to be a log-normal while $P(\zeta)$ and $P(\xi)$ are presumed to be β function PDFs. This model **M4** is to be compared to **M1**.

Model	Flamelets	PDFs	Z-c independent?
M1, Eq. (1)	Unstrained freely propagating premixed	β PDFs for Z and c	Yes
M2, Eq. (1)	Unstrained freely propagating premixed	correlated joint PDFs	No
M3, Eq. (5)	non-premixed	β PDF for Z and lognormal PDF for χ	N.A.
M4, Eq. (15)	Strained Counterflow Reactant-to-Product premixed	β PDF for Z and c and lognormal PDF for ψ_{st}	Yes

Table 1. Summary of flamelets and presumed PDFs used in the modelling

Figure 6 compares the mean reaction rate of c, calculated from the DNS data and using the above four closure models. The results are shown as a radial variation for four axial positions marked in Fig. 1. The DNS values are calculated by averaging $\dot{\omega}_{H_2O}/Y^{Eq}_{H_2O}(Z)$ and the local instantaneous reaction rate $\dot{\omega}_{H_2O}$ is evaluated based on the local temperature and species concentration values as per the chemical mechanism used in the DNS. Thus, the contributions from the scalar dissipation rate related terms in Eq. (3) are not included in the mean reaction rate values shown in Fig. 6. The following observations are made from this figure.

- For the upstream position A-A, the DNS results show a single peak at about $R/D \approx 2$ for the mean reaction rate and there are two peaks for the downstream locations shown in Fig. 6, which are not due to insufficient sampling time. This has been verified

using samples collected over 0.04 ms and 0.2 ms, but the results shown here are for a sampling time of 0.08 ms, which is nearly twice the flow-through time. The inner peak corresponds to rich premixed combustion and the outer peak corresponds to non-premixed combustion [10, 37, 38]. At position B-B, the outer diffusion combustion is weak and this zone is beginning to move away from the inner rich premixed branch. Thus, the outer peak is less obvious compared to the inner peak. However, the relative importance of the outer diffusion combustion increases as one moves downstream. This becomes clear if one compares the inner and outer peak values at a given location. The outer peak is nearly one half of the inner peak for location B1-B1 and these two peaks become nearly of equal magnitude for location C-C. Also, the location of these peak values changes implying the growth of the flame brush in the radial direction as one moves downstream, which is also suggested by the mean temperature field shown in Fig. 1.

- The premixed flamelet models **M1** and **M2** give similar agreement with the DNS values for the position A-A. This is because the covariance, $\overline{c'Z'}$, at this position is small [37] and therefore the approximation of statistical independence of c and Z is acceptable, which is also supported by the joint PDF results in Fig. 5. The mean reaction rate values computed using these two flamelet models are larger than the DNS values for the downstream positions as shown in Fig. 6. However, including the effect of covariance, $\overline{c'Z'}$, in the model **M2** reduces the overestimation and improves the modelled value substantially compared to the model **M1**. The larger values seen for the **M2** model are due to the over-prediction of $\dot{\omega}(\xi, \zeta)$ in premixed flamelets of rich mixture. The flame front thickness in the turbulent flame was shown to be larger than the premixed flamelet thickness by Ruan et al. [37] supporting the above observation on the reaction rate.

- The diffusion flamelet model **M3** gives a broader flame brush (non-zero $\overline{\dot{\omega}_c}$) for the position A-A with considerably lower value for the mean reaction rate. This model values seem to agree reasonably with the DNS values at the outer radial locations for the downstream positions, where the non-premixed combustion is predominant. This is consistent with a previous study [37]. However, this model yields zero reaction rate for the inner regions, where rich premixed combustion occurs. This illustrates the limitation of the non-premixed flamelet model for this lifted flame.

- The extended strained premixed flamelet model, **M4**, significantly underestimates the mean reaction rate for the position A-A. The level of this underestimation improves as one moves in the downstream direction. The turbulence stretch on the flame front is expected to increase with downstream position because of large-scale turbulence resulting from entrainment process and thus the results of **M4** model improve.

Based on the above discussion, the results shown in Fig. 6 and their overall accuracy, and the amount of computational effort involved, it seems that the unstrained premixed flamelets with presumed correlated joint PDF is a reasonable and satisfactory choice to model the turbulent lifted jet flame.

A close study of Eq. (1) shows that the Reynolds PDF is required to calculate the mean reaction rate. This implies that the Reynolds statistics, $\overline{Z}$, $\overline{c}$, $\overline{Z'^2}$, $\overline{c'^2}$ and $\overline{c'Z'}$, are required in the presumed PDF approach and these statistics are unavailable in numerical simulations of turbulent reacting flows since these simulations involve density weighted or Favre averages. It is not always easy to construct Reynolds statistics from Favre statistics and also the presumed PDFs obtained using the mean and variance values from simulations would be the Favre PDFs. This introduces some difficulties in obtaining the joint PDF, $P(\xi, \zeta)$, required for the model **M2**. The relationship between the Favre and Reynolds

PDFs given by $\overline{\rho}\widetilde{P}(\xi) = \rho P(\xi)$ is straight forward to use for a single variate PDF, but it is not so for the joint PDF because the Favre joint PDF cannot be expressed as a product of two Favre PDFs. Here, an approximation $\widetilde{P}(\xi,\zeta) \approx \widetilde{P}(\xi)\widetilde{P}(\zeta)$ is made following earlier studies [56–58] when the statistical independence is assumed, otherwise two marginal Favre PDFs are combined following the method of copula described in section 3.3 to get $\widetilde{P}(\xi,\zeta)$ [40]. Now, the mean reaction rate is calculated using

$$\overline{\dot{\omega}}_c = \bar{\rho}^* \int\int \left[\frac{\dot{\omega}_c(\zeta,\xi)}{\rho(\zeta,\xi)}\right] \widetilde{P}(\zeta,\xi) \quad d\zeta\, d\xi, \tag{16}$$

where $\bar{\rho}^*$ is the mean density obtained from the DNS for this *a priori* assessment. In a numerical simulation, this density will be obtained from the CFD code. The quantities within the square bracket come from the unstrained premixed laminar flamelets. The mean reaction rate calculated using Eq. (16), denoted as M2 Fav, is also shown in Fig. 6. The error introduced by the above approximation of using Favre PDFs is observed to be generally small in regions with significant reaction rate.

3.5 Closure of dissipation rate related terms in Eq. (3)

For the progress variable defined in Eq. (8), the derivatives in Eq. (3) become

$$\frac{\partial Y_{\mathrm{H_2O}}}{\partial Z} = c\,\frac{\mathrm{d}Y^{Eq}_{\mathrm{H_2O}}}{\mathrm{d}Z} \quad \text{and} \quad \frac{\partial^2 Y_{\mathrm{H_2O}}}{\partial Z^2} = c\,\frac{\mathrm{d}^2 Y^{Eq}_{\mathrm{H_2O}}}{\mathrm{d}Z^2},$$

$$\frac{\partial Y_{\mathrm{H_2O}}}{\partial c} = Y^{Eq}_{\mathrm{H_2O}}(Z), \quad \frac{\partial^2 Y_{\mathrm{H_2O}}}{\partial c^2} = 0 \quad \text{and} \quad \frac{\partial^2 Y_{\mathrm{H_2O}}}{\partial Z \partial c} = \frac{\mathrm{d}Y^{Eq}_{\mathrm{H_2O}}}{\mathrm{d}Z}. \tag{17}$$

Substituting these derivatives into Eq. (3) one gets

$$\overline{\dot{\omega}}^*_c = \underbrace{\overline{\dot{\omega}}_c}_{\text{(I)}} + \underbrace{\overline{\rho \frac{c}{Y^{Eq}_{\mathrm{H_2O}}(Z)} \frac{\mathrm{d}^2 Y^{Eq}_{\mathrm{H_2O}}}{\mathrm{d}Z^2} N_{ZZ}}}_{\text{(II)}} + \underbrace{\overline{2\rho \frac{1}{Y^{Eq}_{\mathrm{H_2O}}(Z)} \frac{\mathrm{d}Y^{Eq}_{\mathrm{H_2O}}}{\mathrm{d}Z} N_{cZ}}}_{\text{(III)}}. \tag{18}$$

There are two extra terms, (II) and (III), contributing to the overall mean reaction rate in partially premixed combustion. These additional contributions include effects of turbulent mixing at small scales and chemical kinetics. The turbulent mixing is felt through N_{ZZ} and N_{cZ} and the chemical kinetics effects come through the first and second derivatives with respect to Z. The term (II) signifies contribution from the non-premixed burning mode and is expected to contribute predominantly near the stoichiometric mixture fraction. The contribution from correlation between the gradients of Z and c is denoted by the term (III) in Eq. (18).

The chemical kinetics terms are shown in Fig. 7 by plotting the variation of $\Psi = Y^{Eq}_{\mathrm{H_2O}}$, $\Psi' = \mathrm{d}\Psi/\mathrm{d}Z$ and $\Psi'' = \mathrm{d}^2\Psi/\mathrm{d}Z^2$ with Z. These values are obtained by performing equilibrium calculations by allowing the species involved in the chemical kinetic mechanism used in the DNS to be present in the equilibrium mixture. There are large changes in Ψ' and Ψ'' close to the stoichiometric value, $Z_{st} = 0.03$, as one would expect. The first derivative is positive for $Z < 0.04$, zero for $Z = 0.042$ and approaches a value of about -0.275 for $Z > 0.07$. The second derivative is negative reaching a peak at Z_{st} and approaching zero for $Z < 0.015$ and $Z > 0.05$ and thus the term (II) will contribute only in this narrow range around stoichiometry. Also, the second derivative is nearly 100 times larger than the first

derivative and thus the contribution of term (II) is expected to be larger than term (III). The contribution of term (III) is expected only for $Z < 0.042$ and this will be compounded by the behaviour and magnitude of the cross dissipation rate, N_{cZ}. It was shown in [37] that the cross dissipation rate is an order of magnitude smaller than the mixture fraction dissipation rate and thus the contribution of term (III) is expected to be negligible.

Previous analyses of N_{cZ} in stratified [59] and partially premixed combustion [37] using the respective DNS data have shown that N_{cZ} is an order of magnitude smaller than N_{ZZ}. Furthermore, Fig. 7 shows that the first derivative involved in term (III) is an order of magnitude smaller than the second derivative involved in term (II). Also, the term (III) is estimated to be less than 1% of the term (I) and thus the term (III) is neglected in this study following previous studies [14, 22, 25]. The effect of the mixture fraction dissipation rate on the overall mean reaction rate was also noted by Müller et al. [17] in partially premixed combustion modelling using the G-equation approach. They modelled the turbulent flame speed so that it decreased as N_{ZZ} increased. In the current study, no such approximation is made and the contributions from the three dissipation rates occur naturally.

The term (II) requires modelling and non-premixed flamelets have been used in the past [14], but that approach required solution to a transport equation for burning mode indicator which involves further complex modelling. Here, a simple algebraic model is explored, as a first approximation, to ease the computational and further modelling burdens. This model is written as written as

$$\overline{\rho \frac{c}{Y^{Eq}_{\mathrm{H_2O}}(Z)} \frac{\mathrm{d}^2 Y^{Eq}_{\mathrm{H_2O}}}{\mathrm{d}Z^2} N_{ZZ}} \;\simeq\; \overline{\rho}\,\widetilde{c}\,\widetilde{\epsilon}_{ZZ} \int_{\xi_{st}-\Delta\xi}^{\xi_{st}+\Delta\xi} \frac{1}{Y^{Eq}_{\mathrm{H_2O}}(\xi)} \frac{\mathrm{d}^2 Y^{Eq}_{\mathrm{H_2O}}(\xi)}{\mathrm{d}Z^2} \widetilde{P}_\beta(\xi)\; d\xi, \qquad (19)$$

where $\widetilde{\epsilon}_{ZZ}$ is the scalar dissipation rate and it will be defined and discussed later in Section 4.1. Since the second derivative is significant only around the stoichiometry, $\Delta\xi$ is set to be a constant of 0.02, which is consistent with Müller et al. [17]. They considered the effect of N_{ZZ} on turbulent burning velocity to be important only in the range of Z for which the laminar flame speed is a significant fraction of its value at stoichiometry.

Figure 8 compares the model values given by Eq. (19) with the DNS results (left hand side of Eq. (19)) for three axial positions. Although the general trend is captured quite well this model overestimates the magnitude. The level of this overestimation is large for the upstream position A-A and it reduces with downstream distance. The overestimation is mainly in the region where the mixture is rich. The location of peak value is captured reasonably well except for the position B-B, the model peak is at $R/D = 2.5$ but the DNS result has a peak at $R/D = 2.8$. This shift is because of the influence of $\widetilde{\epsilon}_{ZZ}$ behaviour at this position. A comparison of the results in Fig. 8 to those in Fig. 6 suggests that the contribution from the non-premixed mode term (II) cannot be neglected in comparison to term (I) of Eq. (18), especially in the outer region of the flame brush at downstream position. For example, at B-B $R/D = 2.7$ and C-C $R/D = 3.6$, term (II) is about 30% of term (I), which cannot be ignored. Thus, the contribution given by Eq. (19) must be included in the calculations of lifted flames or partially premixed flames in general.

To summarise the *a-priori* assessment, the flamelets model **M2** along with the correlated Favre PDF seem to be a good choice to model the term (I) of Eq. (18) on the balance among the ease of implementation, computational effort required and, accuracy and consistency of the solution. The contribution of the non-premixed mode given by Eq. (19) cannot be ignored on the physical grounds. Thus, the model **M2** and Eq. (19) are used for *a posteriori* validation discussed in the next section.

4. *A posteriori* validation using RANS simulation

The governing equations and their modelling are discussed first. This is followed by a discussion on implementation of the combustion model identified in the previous section. A commercial CFD code, Fluent, is used for the turbulence and flow modelling, and the combustion model is implemented using UDFs (user defined functions) and UDMs (user defined memory). Detail on this is also presented in this section along with boundary conditions used. The transport equations included through UDS (user defined scalars) are identified in the discussion below. It is worth noting that the combustion models available in the Fluent are not used in this study.

4.1 Governing equations

The equations for conservation of mass, momentum and enthalpy solved are

$$\frac{\partial \overline{\rho}}{\partial t} + \frac{\partial \overline{\rho}\,\widetilde{u}_i}{\partial x_i} = 0, \tag{20}$$

$$\frac{\partial \overline{\rho}\,\widetilde{u}_i}{\partial t} + \frac{\partial \overline{\rho}\,\widetilde{u}_i\widetilde{u}_k}{\partial x_k} = -\frac{\partial \overline{p}}{\partial x_i} + \frac{\partial}{\partial x_k}\left(\overline{\tau_{ik}} - \overline{\rho}\,\widetilde{u_i''u_k''}\right), \tag{21}$$

$$\frac{\partial \overline{\rho}\,\widetilde{h}}{\partial t} + \frac{\partial \overline{\rho u}_k\,\widetilde{h}}{\partial x_k} = \frac{\partial}{\partial x_k}\left[\overline{\frac{\mu}{S_C}\frac{\partial h}{\partial x_k}} - \overline{\rho u_k'' h''}\right], \tag{22}$$

respectively. The standard nomenclature is used for the above equations and the symbol S_C denotes the molecular Schmidt number for the enthalpy.

The two equation, $\widetilde{k}$-$\widetilde{\varepsilon}$, modelling approach of Jones and Launder [60] is used for turbulence modelling as it is widely used due to its simplicity, low computational cost and reasonable accuracy for a wide range of flow configurations. The turbulent kinetic energy is denoted by $\widetilde{k}$ and its dissipation rate is $\widetilde{\varepsilon}$. Their equations are written as [61]

$$\frac{\partial \overline{\rho}\,\widetilde{k}}{\partial t} + \frac{\partial \overline{\rho}\,\widetilde{u}_i\,\widetilde{k}}{\partial x_i} = \frac{\partial}{\partial x_j}\left[\left(\mu + \frac{\mu_t}{S_{Ck}}\right)\frac{\partial \widetilde{k}}{\partial x_j}\right] + P_k - \overline{\rho}\,\widetilde{\varepsilon}, \tag{23}$$

$$\frac{\partial \overline{\rho}\,\widetilde{\varepsilon}}{\partial t} + \frac{\partial \overline{\rho}\,\widetilde{u}_i\,\widetilde{\varepsilon}}{\partial x_i} = \frac{\partial}{\partial x_j}\left[\left(\mu + \frac{\mu_t}{S_{C\varepsilon}}\right)\frac{\partial \widetilde{\varepsilon}}{\partial x_j}\right] - C_{\varepsilon 1}\frac{\widetilde{\varepsilon}}{\widetilde{k}}P_k - C_{\varepsilon 2}\overline{\rho}\,\frac{\widetilde{\varepsilon}^2}{\widetilde{k}}, \tag{24}$$

$$P_k = -\overline{\rho}\,\widetilde{u_i''u_j''}\,\frac{\partial \widetilde{u}_i}{\partial x_j} - \overline{u_i''}\frac{\partial \overline{p}}{\partial x_i} + \overline{p'\frac{\partial u_i''}{\partial x_i}}. \tag{25}$$

The pressure dilatation term in Eq.(25) is closed using the model in [62]. The influence of this term is small for the test case since it is an open flame. The turbulent eddy viscosity is calculated using $\mu_t = C_\mu\,\overline{\rho}\,\widetilde{k}^2/\widetilde{\varepsilon}$ with $C_\mu = 0.09$, $C_{\varepsilon 1} = 1.44$ and $C_{\varepsilon 2} = 1.92$ are standard model constants. These constants, except for $C_{\varepsilon 2} = 1.96$ as explained in Sec 4.3, are used in this study.

The lifted hydrogen jet flames investigated experimentally in [47, 48, 63] have been simulated using the CMC method in earlier studies [28, 29]. The main challenge in simulating these flames is to obtain the lift-off height correctly. Here, the flamelets based method, identified as **M2** in the previous section along with Eq. (19) is used to close the mean reaction rate given by Eq. (18). Thus, transport equations for $\widetilde{Z}$, $\widetilde{Z''^2}$, $\widetilde{c}$, $\widetilde{c''^2}$ and the covariance $\widetilde{c''Z''}$ need to be solved. These equations are [64, 65]

$$\frac{\partial \overline{\rho}\,\widetilde{Z}}{\partial t} + \frac{\partial \overline{\rho}\,\widetilde{u}_k\,\widetilde{Z}}{\partial x_k} = \frac{\partial}{\partial x_k}\left(\overline{\rho D \frac{\partial Z}{\partial x_k}} - \overline{\rho\, u_k'' Z''}\right), \tag{26}$$

$$\frac{\partial \overline{\rho}\,\widetilde{Z''^2}}{\partial t} + \frac{\partial \overline{\rho}\,\widetilde{u}_k\,\widetilde{Z''^2}}{\partial x_k} = \frac{\partial}{\partial x_k}\left(\overline{\rho D \frac{\partial Z''^2}{\partial x_k}} - \overline{\rho\, u_k'' Z''^2}\right) - 2\,\overline{\rho}\,\widetilde{\epsilon}_{ZZ} - 2\,\overline{\rho\, u_k'' Z''}\frac{\partial \widetilde{Z}}{\partial x_k}, \tag{27}$$

$$\frac{\partial \overline{\rho c}}{\partial t} + \frac{\partial \overline{\rho}\,\widetilde{u}_k\,\widetilde{c}}{\partial x_k} = \frac{\partial}{\partial x_k}\left(\overline{\rho D \frac{\partial c}{\partial x_k}} - \overline{\rho\, u_k'' c''}\right) + \overline{\dot{\omega}}_c^*, \tag{28}$$

$$\frac{\partial \overline{\rho}\,\widetilde{c''^2}}{\partial t} + \frac{\partial \overline{\rho}\,\widetilde{u}_k\,\widetilde{c''^2}}{\partial x_k} = \frac{\partial}{\partial x_k}\left(\overline{\rho D \frac{\partial c''^2}{\partial x_k}} - \overline{\rho\, u_k'' c''^2}\right) - 2\,\overline{\rho}\,\widetilde{\epsilon}_{cc} - 2\,\overline{\rho\, u_k'' c''}\frac{\partial \widetilde{c}}{\partial x_k} + 2\,\overline{c''\dot{\omega}_c''}, \tag{29}$$

and $$\frac{\partial \overline{\rho}\,\widetilde{c''Z''}}{\partial t} + \frac{\partial \overline{\rho}\,\widetilde{u}_k\,\widetilde{c''Z''}}{\partial x_k} = \frac{\partial}{\partial x_k}\left(\overline{\rho D \frac{\partial c''Z''}{\partial x_k}} - \overline{\rho u_k'' c''Z''}\right) - 2\,\overline{\rho}\,\widetilde{\epsilon}_{cZ} - \overline{\rho\, u_k'' c''}\frac{\partial \widetilde{Z}}{\partial x_k} - \overline{\rho\, u_k'' Z''}\frac{\partial \widetilde{c}}{\partial x_k} + \overline{Z''\dot{\omega}_c''}. \tag{30}$$

The various turbulent scalar fluxes are modelled using a gradient flux approximation, for example $\widetilde{u_k'' Z''} = -D_t \partial \widetilde{Z}/\partial x_k$ with a turbulent diffusivity D_t. The turbulent scalar flux of c can become counter gradient under appropriate condition, which can also be modelled using a second order closure. Here, a gradient flux approximation is used to eliminate the uncertainties that could arise through the second order modelling. Furthermore, this scalar flux is known to be gradient in turbulent premixed combustion at high Reynolds number.

The source term $\overline{\dot{\omega}}_c^*$ in equation (28) is given by Eq. (18), which is closed as noted in the previous section. The Favre averaged dissipation rate of the mixture fraction fluctuation is modelled as

$$\overline{\rho}\,\widetilde{\epsilon}_{ZZ} = \overline{\rho D_Z (\nabla Z'' \cdot \nabla Z'')} \simeq C_d\,\overline{\rho}\left(\frac{\widetilde{\varepsilon}}{\widetilde{k}}\right)\widetilde{Z''^2}, \tag{31}$$

assuming a proportionality between scalar and turbulence time scales [66] and $C_d \approx 1$ is

a model constant. A similar algebraic model is used for the cross dissipation rate

$$\overline{\rho}\,\widetilde{\epsilon}_{cZ} = \overline{\rho D_Z(\nabla c'' \cdot \nabla Z'')} \simeq C_{cZ}\,\overline{\rho}\left(\frac{\widetilde{\varepsilon}}{\widetilde{k}}\right)\widetilde{c''Z''}, \tag{32}$$

with $C_{cZ} = 1$ [37].

A simple algebraic model exists for $\widetilde{\epsilon}_{cc}$ in a form similar to Eq. (31), which is known to be insufficient [67, 68]. So, Kolla et al. [69] proposed a new model based on the physics of reactive scalar mixing in premixed flames, which was subsequently modified to include the mixture fraction variation [70]. This model is

$$\overline{\rho}\,\widetilde{\epsilon}_{cc} = \overline{\rho D(\nabla c'' \cdot \nabla c'')} \simeq \frac{\overline{\rho}}{\beta'}\left([2K_c^* - \tau(Z)C_4]\,\frac{S_L^0(Z)}{\delta_L^0(Z)} + C_3\frac{\widetilde{\varepsilon}}{\widetilde{k}}\right)\widetilde{c''^2}, \tag{33}$$

with

$$C_3 = \frac{1.5\sqrt{\mathrm{Ka}}}{1+\sqrt{\mathrm{Ka}}} \quad \text{and} \quad C_4 = 1.1(1+\mathrm{Ka})^{-0.4}, \tag{34}$$

where $\beta' \simeq 6.7$ was derived from DNS of fully premixed flames [71]. The hydrogen-air laminar planar flame calculations suggested that $K_c^*/\tau \approx 0.65$ is a good approximation for the stoichiometric and rich hydrogen-air flames [72]. The parameter $\tau(Z) = (T_b(Z) - T_u)/T_u$ is the normalised temperature rise, with the subscripts b and u indicating burnt and unburnt states. The unstrained laminar flame speed and its thermal thickness for a mixture having the mixture fraction value of Z are denoted respectively as $S_L^0(Z)$ and $\delta_L^0(Z)$. The Karlovitz number, Ka, is defined as

$$\mathrm{Ka} \equiv \frac{t_c}{t_k} \simeq \frac{\delta(Z)/S_L^0(Z)}{\sqrt{\nu/\widetilde{\varepsilon}}}, \tag{35}$$

where t_k is the Kolmogorov time scale, t_c is the chemical time scale defined as δ/S_L^0 with δ as the Zeldovich flame thickness which is related to the thermal thickness through $\delta_L^0(Z)/\delta(Z) \approx 2(1+\tau(Z))^{0.7}$, and ν is the kinematic viscosity. In Eq.(33)-(35), the local value of $\widetilde{Z}$ is used for simplicity. Also, c has to be defined using a species having Lewis number close to unity for the model in Eq. (33) to work satisfactorily since its development is based on unity Le approximation. Thus, c is defined using water vapour mass fraction for this study as noted earlier.

The chemical source terms in Eqs. (29) and (30) are modelled as

$$\overline{c''\dot{\omega}_c''} \approx \overline{c''\dot{\omega}_c} = \overline{\rho}\int_0^1\int_0^1 \left(\zeta - \widetilde{\zeta}\right)\frac{\dot{\omega}_c(\xi,\zeta)}{\rho(\xi,\zeta)}\,\widetilde{P}(\xi,\zeta)\quad d\xi\;\; d\zeta, \tag{36}$$

$$\overline{Z''\dot{\omega}_c''} \approx \overline{Z''\dot{\omega}_c} = \overline{\rho}\int_0^1\int_0^1 \left(\xi - \widetilde{\xi}\right)\frac{\dot{\omega}_c(\xi,\zeta)}{\rho(\xi,\zeta)}\,\widetilde{P}(\xi,\zeta)\quad d\xi\;\; d\zeta, \tag{37}$$

The temperature is calculated using the total enthalpy $\widetilde{h}$ computed in the simulation using Eq. (22). This includes the sensible and chemical parts as

$$\widetilde{h} = c_{p,\mathrm{mix}}(\widetilde{T} - T_0) + \Delta h^0_{f,\mathrm{mix}}, \tag{38}$$

where $T_0 = 298$ K is a reference temperature. The mixture averaged specific heat capacity $c_{p,\mathrm{mix}}$, the enthalpy of formation $\Delta h^0_{f,\mathrm{mix}}$ and the mixture molecular weight W_{mix} required for the state equation are calculated as follows.

$$c_{p,\mathrm{mix}} = \int_0^1 \int_0^1 c_p^e(\xi,\zeta)\, \widetilde{P}(\xi,\zeta) \quad d\zeta \quad d\xi, \tag{39}$$

$$\Delta h^0_{f,\mathrm{mix}} = \sum \int_0^1 \int_0^1 Y_i\, \Delta h^0_{f,i}\, \widetilde{P}(\xi,\zeta) \quad d\zeta \quad d\xi, \tag{40}$$

$$W_{\mathrm{mix}} = \int_0^1 \int_0^1 \left(\sum (Y_i/W_i)\right)^{-1} \widetilde{P}(\xi,\zeta) \quad d\zeta \quad d\xi. \tag{41}$$

The $c_{p,mix}$ given by Eq.(38) includes its temperature dependence through Eq.(39) while simulating the turbulent combustion. An effective specific heat capacity, defined as $c_p^e = \left(\int_{T_0}^{T_1} c_p\, dT\right) / (T_1 - T_0)$ is used to include the temperature dependence at the flamelets level. T_1 is the local temperature at which c_p^e is calculated in flamelet .

Figure 9 illustrates the calculation procedure for the above equations, Eqs. (39) to (41). The laminar unstrained planar flame quantities are used when the mixture fraction value is within the lean, Z_l, and rich, Z_r, flammability limits. Outside this range, either the air or fuel properties are interpolated with the laminar flame values appropriately before the double integrations in the above equations are performed.

The above quantities together with the mean mass fractions, $\overline{\dot{\omega}_c}$, $\overline{c''\dot{\omega}''_c}$ and $\overline{Z''\dot{\omega}''_c}$ are tabulated with $\widetilde{Z}$, $\widetilde{c}$, $\widetilde{Z''^2}$, $\widetilde{c''^2}$ and $\widetilde{c''Z''}$ as controlling variables. This table is used in RANS simulation to supply the required quantity. The temperature, $\widetilde{T}$, depends on $\widetilde{Z}$, $\widetilde{c}$, $\widetilde{Z''^2}$, $\widetilde{c''^2}$, and $\widetilde{c''Z''}$ through Eq. (38). The mixture mean density, $\overline{\rho}$, is related to temperature through the equation of state. The temperature and density are calculated during the simulation.

The transport equations for mass, momentum, energy and turbulence given in Eqs. (20) to (24) are to be solved for all the models. Thus, the computational cost for the four models in Table 1 depends on the additional transport equations required and the computations involved in generating and using the look-up tables. The model **M1** requires four additional transport equations, Eqs. (26) to (29), and four dimensional look-up table is involved. The model **M2** is slightly more expensive than **M1** because it involves five dimensional look-up table and an additional transport equation in Eq. (30). The model **M3** is the least expensive as it involves only two additional transport equations, Eqs. (26) and (27), and a two dimensional look-up table. The model **M4** involves the same number of equations and five dimensional look-up table as for **M2**, but the look-up table generation involves significant additional computations as it involves strained flamelets. Thus, overall **M4** is the most computationally expensive model. If one compares the computational time for turbulent flame simulation part only after excluding the expenses involved in generating look-up table then the models **M1**, **M2** and **M3** are on par with one another and the model **M3** is the least expensive. A typical simulation of the lifted flame considered here using **M2** took about 48 hours of wall-clock time in a desktop having a memory of 8GB and 3 CPUs running at 2GHz.

Although **M3** is the least expensive model, the results of *a priori* assessment in Fig.6 show that this model cannot capture the mean reaction rate variation, specifically the contribution coming from the premixed part, reasonably. The model **M4** tend to greatly underestimate the mean reaction rate in flame stabilisation region and it is the most expensive

model. For these reasons, the models **M1** and **M2** are used for the *posteriori* assessment conducted in this section.

4.2 Model Implementation

Figure 10 presents a schematic of the computational domain for a 2D axisymmetric model of the turbulent lifted jet flame investigated experimentally in [47, 48, 63]. The computational grid contains about 30000 quadrilateral cells, and extends to 50D in radial, r, and 200D in axial, y, directions. The jet nozzle diameter is $D = 2$ mm. Two meshes, a coarse mesh with 13800 cells and a fine mesh with 30000 cells resulting from refinement in the shear layer regions, were used in the simulations. These simulations showed a negligible variation in the results, to be presented later, and thus the results for the fine grid are shown in this paper.

A 5 dimensional look-up table is used for the simulations. The number of points in this table are 24, 21, 16, 16, 11 in $\widetilde{Z}$, $\widetilde{c}$, normalised $\widetilde{Z''^2}$, $\widetilde{c''^2}$ and $\widetilde{Z''c''}$ directions respectively. These points are unevenly distributed to ensure good resolution for mixtures close to stoichiometric, $\widetilde{Z}$ space, and near $\widetilde{c} \approx 0.7$ where reaction tends to be large. Linear interpolation is used in each of these 5 dimensions and the interpolation error in region with substantial reaction rate is estimated to be around 1%.

4.2.1 Boundary Conditions

The various boundary conditions used in the simulation are also marked in Fig. 10. The jet and entrainment boundary have mass-flow-inlet boundary conditions. The inlet velocity profile in the jet is prescribed using a 1/7 power law with a bulk mean velocity of 680 m/s as used for the DNS calculation [10]. Turbulent intensity is set to be 5% with a turbulence integral length scale of 2 mm [28]. The mixture fraction is 1.0 and the enthalpy is -258460 J/kg for hydrogen at 280 K at the jet exit. All other scalars have zero values at the jet exit.

The mass flow rate at the entrainment boundary is specified according to Spalding [73] using

$$\frac{\mathrm{d}\dot{m}}{\mathrm{d}r} \approx 0.28\,\rho_{\mathrm{air}}^{0.5} F^{0.5} \quad \text{with} \quad F = \rho_j U_j^2 \pi r_j^2, \tag{42}$$

where $\dot{m}$ is the entrained mass flow rate and the subscript j denotes jet exit values. A small constant entrainment velocity of 0.1 m/s has also been tested and results were found to have no significant difference. Turbulent intensity is set to a low value of 0.001% for this boundary. The enthalpy of air at 298 K and zero for all other scalars are used on this boundary. The no-slip wall boundary used for the far stream helps to stabilise the calculation. At the wall boundary, the enthalpy of ambient air is used and zero values are set for all other scalars. At the flow exit, a pressure outlet boundary condition with zero axial gradient for the scalars is used.

4.2.2 Fluent UDF and UDS

A pressure based incompressible flow solver in Fluent was used in this study. This may introduce some errors in the flow field when the compressibility effects become important since the jet Mach number is 0.54. The density based compressible flow solver in Fluent is also used to compute the non-reacting flow field for the case of interest for this study and the difference in the mean and fluctuating velocities computed using these two solvers are found to be less than 1%. Furthermore, the flame is expected to stabilise in regions of low velocity and thus the influence of compressibility effects on the flame structure and stabilisation is expected to be negligible. Thus, the overall conclusions of this study will not change if a compressible solver is used.

The SIMPLE algorithm is used to couple pressure and velocity fields. The transport equations, except for the mass, momentum and turbulence, for six additional scalars, $\widetilde{Z}$, $\widetilde{Z''^2}$, $\widetilde{c}$, $\widetilde{c''^2}$, $\widetilde{c''Z''}$ and $\widetilde{h}$, with various sources and sinks noted earlier in this section were solved as UDS. These sources and sinks were included using UDFs. Figure 11 presents a flow chart for the steps involved in the calculation procedure. The procedures enclosed inside dashed lines have been developed in this work. The temperature and density fields are calculated at each iteration through respective UDFs. It is worth noting that Fluent solves the flow and turbulence equations as for an isothermal non-reacting case and no default energy equation or Fluent's combustion models are used. The combustion effect is coupled to the flow field through density variation which is computed through UDS and UDFs. This gives full control on the combustion modelling related equations and their solutions.

4.2.3 Flame kernel initialisation

First a non-reacting flow was computed. A small flame kernel was then initialised by setting one or two cells with $\widetilde{c} = 1.0$ and $\widetilde{h} = -36871$ J/kg, corresponding to burnt products of stoichiometric hydrogen-air mixture, at a radial position where $\widetilde{Z} = Z_{\rm st}$. The flame kernel was then allowed to evolve and reach a final lift-off height. Two different sizes of 0.3×1.0 and 0.7×0.75 squared mm for the kernels with an energy content of about 1.3 mJ and 2.6 mJ respectively. were tested. These energies are substantially larger than the minimum ignition energy of 0.02 mJ required for stoichiometric hydrogen-air mixture [74, pp.488]. Also, two axial positions, 9D and 12D chosen arbitrarily, have been tested for this initialisation. The final lift-off height was found to be insensitive to the initial location of the flame kernel.

4.3 Results and Discussions

A comparison of the computed and measured [47] mixture fraction statistics, as has been done in previous studies [28, 29], is shown in Fig. 12 for $y = 7D$ and $9.5D$ positions. The mean and RMS values are normalised by the respective centreline values. A reasonable agreement between RANS and experimental results is observed in Fig. 12. As noted earlier, the model parameter $c_{\varepsilon 2}$ is increased slightly ($c_{\varepsilon 2} = 1.96$) to provide an overall improved agreement as has been done in previous studies [28, 29], This increases the turbulent viscosity, however, it does not impart undue alteration to the spatial diffusion of various quantities computed. A similar observation was made in previous studies of lifted flames using CMC methodology [28, 29]. Details on the CMC methodology can be found in those references.

The Reynolds stress transport model (RSM) with linear pressure-strain term and standard model constants is also used in this study to test for the sensitivity to the turbulence modelling. As one observes in Fig. 12, there is no significant difference between $\widetilde{k}$-$\widetilde{\varepsilon}$ and RSM results and it is known that the computational expenses for the RSM model are significantly larger. Thus the results obtained using $\widetilde{k}$-$\widetilde{\varepsilon}$ model are presented for the following discussion.

4.3.1 Flame brush structure

The lift-off height based on the leading edge of $T = 900$ K isoline, as used in the experiment [63] and CMC calculation [29], is $7.5D$ in this study when the model **M2** and Eq. (19) for term (II) are used. This agrees reasonably well with the experimental observation [47] of $7D$. Thus, it is possible to make a direct and unambiguous comparison of the computed and measured flame brush structure.

The computed radial variations of temperature and mole fractions of H_2, O_2, OH, H_2O and N_2 are compared with measured values for axial positions of $7D$, $9.5D$, and $50D$ in

Figs. 13 to 15 respectively. The results of CMC calculations by Devaud and Bray [28] for $y = 7D$ and by Kim and Mastorakos [29] for $y = 9.5D$ positions are included in Figs. 13 and 14 respectively for comparison. Note that the radial variation of temperature for $y = 9.5D$ from the CMC calculation is not reported in [29] and thus it is not shown in Fig. 14.

The peak value of the temperature for $y = 7D$, shown in Fig. 13, calculated using the current models is about 650 K compared to 900 K observed in the experimental study [47], while the CMC calculation [28] gives higher values. This is due to the small difference in lift-off height, $7.5D$ in the current study and $7D$ in the experiment [47] based on the most leading edge of 900 K iso-contour. This gives a lower temperature and slightly higher H_2, lower OH and H_2O mole fractions since the flame at $7D$ is not as fully established as that in the experiment. The temperature and species variation at the lift-off height of $7.5D$ is also included in Fig. 13. The agreement between computed, ($y = 7.5D$) and experimental values, specifically for temperature, X_{OH}, X_{H2O} and X_{O2} is good. The variations resulting from CMC calculation seem broader implying a slightly broader flame brush, which can be seen clearly in temperature, OH and H2O variations shown in Fig. 13. Nevertheless, the results of these two models are comparable and the flamelets model has a lower computational cost.

In Fig. 14, the combustion model used in this study gives some under-prediction for temperature and, OH and H_2O mole fractions for $R/D < 3$. There is a consistent over-prediction of H_2 and O_2 in this region as one observes in Fig. 14. The agreement between the experimental data and the computational results from this study is good for $R/D \geq 3$. The disagreement for $R/D < 3$ is because the mixture there is rich, which can be beyond the rich flammability limit. The scalar mole fractions computed using the flamelets model in this study and those reported in [29] for CMC are comparable and their agreement with the measured values is satisfactory. It is worth noting that the drop in O_2 mole fraction observed in the experiment near $R/D = 2$ is captured by the flamelets model used in this study. In general, both the CMC and flamelets based model yield similar results.

The comparison of computed and measured values for a far downstream position of $y = 50D$ is shown in Fig. 15. The agreement is reasonable except for $R/D < 3$, which is again due to combustion of very rich mixture. It is known that flamelet models have their limitations for chemical kinetics dominated fuel-rich combustion. However, the overall agreement is reasonable for the current modelling approach in general. A similar level of comparison is seen for other downstream positions [75].

4.3.2 Flame lift-off height

Predicting the flame lift-off height as a function of jet velocity is challenging for the reasons noted in section 1. Before presenting this result in this subsection, the effects of various modelling, *Z-c* correlation and contribution of non-premixed combustion, on the flame lift-off height is discussed first. The premixed flamelets models **M1** and **M2** are considered with and without the contribution of non-premixed combustion, term (II) in Eq. (19). The various combinations of these models are summarised in Table 2 along with the corresponding flame lift-off heights computed in this study.

Case	A	B	C	D
Combus. model	**M1**	**M1** + term (II)	**M2**	**M2** + term (II)
Lift-off Height (h/D)	4.5	5.2	6	7.5

Table 2. Flame lift-off height for various model combinations.

Figure 16 shows the mean temperature field and mixture fraction contours for the four cases listed in Table 2. Just to remind ourselves, the flamelets model **M1** does not include *Z-c* correlation whereas the model **M2** includes the correlation as noted in Table 1. The lift-off height, h/D, noted in Table 2 is based on the most leading edge of $T = 900$ K

and it is $4.5D$ for Case-A. This value is less than $7D$ observed in the experiment [47]. When the contribution of non-premixed mode combustion is included through Eq. (19), the flame lift-off height increases to $5.2D$, but still smaller than the experimental value, as shown in Fig. 16(b) for the Case-B in Table 2. If one includes *Z-c* correlation without the term (II), Case-C in Table 2, then the lift-off height increases to $6D$. If the non-premixed combustion contribution is included along with the correlation as for the Case-D then the lift-off height becomes $7.5D$, which is close to the experimental value. Thus, it is clear that the effects of *Z-c* correlation and non-premixed combustion must be captured to get the correct lift-off height.

The effect of including *Z-c* correlation in $\overline{\dot{\omega}_c}$ is shown in Fig. 17 by plotting the pseudo-colour map of $\overline{\dot{\omega}_c}$ for the Case-A and Case-C along with the contour of $\widetilde{Z} = Z_{\rm st}$. Including this correlation in Case-C reduces the mean reaction rate leading to an increase in the lift-off height. The lean and rich branches are distinct in the Case-A which does not include the correlation and these two branches merge in the Case-C. The leading edge becomes more rounded and is shifted to the lean side when the correlation is included.

It has been noted in Fig. 5 that the *Z-c* correlation is small near the flame stabilisation region, but Figs. 16 and 17 clearly show that this correlation influences the lift-off height. Thus, an explanation is required since the results in these figures seem contradictory. At the leading edge of the flame kernel, chemical reaction is small. It is also to be noted that the fluctuation in c is produced by chemical reaction and thus c'' is small near the leading edge, which contributes to the small *Z-c* correlation at this position. However, this leading edge is supported by intense reaction behind it and, the magnitude of this reaction and its location are strongly influenced by *Z-c* correlation as seen in Fig. 17. Thus, the flame-lift off height is influenced by this correlation, which can be seen clearly in Figs. 16 and 17 (also compare Figs. 16a and 16c).

The effects of including non-premixed combustion mode on the overall mean reaction rates can be understood by comparing the total reaction rate $\overline{\dot{\omega}}_c^*$ shown in Fig. 18(a) for the Case-D to that shown in Fig. 17(b) for the Case-C. The maximum value of the mean reaction rate is reduced by about 10% and intense reaction zone present at the leading edge is split into a rich and lean zone in the Case-D. The leading edge is shifted further downstream. The lean and rich branches are merged together even for $y > 16D$ when the non-premixed contribution is included. To gain further understanding, one can plot the different components $\overline{\dot{\omega}}_c$, shown in Fig. 18(b), and the non-premixed component term (II) shown in Fig.18(c). The non-premixed component is large along the stoichiometric contour as one would expect and this contribution is negative, which is responsible for splitting the leading intense reaction zone into a lean and rich part as in Fig. 18(a). This contributions also shift the leading edge downstream. Thus, the effects of *Z-c* correlation and non-premixed combustion play important role on flame lift-off. To test this further, the lift-off height for various jet velocities are computed using the same model. These results are discussed next.

A. Lift-off height vs jet velocity

Figure 19 compares the variation of flame lift-off height with jet velocity from experiments and RANS simulations of this study. The experiment with inlet velocity of 680 m/s has been studied independently by Cheng et al. [47, 48] and Brockhinke et al. [63]. Cheng et al. reported detailed scalar measurements which are used in the earlier part of this section to validate flame brush structure and they did not change the jet exit velocity, whereas Brockhinke et al. [63] varied the jet velocity and reported the corresponding flame lift-off heights but not the flame brush structure. Also, the turbulence conditions at the nozzle exit were not reported in [63]. This creates some difficulties for simulations. One cannot use the commonly adopted correlation for fully developed pipe

flow to specify the turbulence level based on flow Reynolds number. This is because the balance between pressure gradient and viscous terms, expected for a fully developed pipe flow, does not hold at the nozzle exit because of the discontinuity in the nozzle wall. This forced a systematic variation of the turbulence level at the fuel jet exit to assess the lift-off height sensitivity to the inlet turbulence level. Indeed, the calculated lift-off height is found to be sensitive to the inlet turbulence because the flow and scalar mixing behaviour in the near field of the jet are bound to depend on the jet exit condition. The flame stabilisation strongly influenced by the flow and mixing fields is invariably in the jet near field and thus the lift-off height is sensitive to the turbulence level at the fuel jet exit. In this study, the turbulence intensity of 25% for 500 m/s, 15% for 590 m/s, and 0.1% for 850 m/s are used for the results shown in Fig. 19. The turbulence intensity for the 680 m/s case was specified to be 5% as noted earlier in subsection 4.2.1 based on the experimental value [47, 48]. The flame lift-off height for the 680 m/s case reported in [47, 48] and [63] differs by about $1.5D$ as shown in Fig. 19 and the simulation result falls between these two experimental values. The agreement between the computed and measured lift-off height as function of jet velocity is very good as one observes in Fig. 19. This further confirms the earlier observation on the role of Z-c correlation and non-premixed combustion contribution.

B. Flame stabilisation mechanism

The mechanism of flame stabilisation in a lifted flame is still a open question [2, 3, 7] and its detailed discussion is beyond the scope of this paper. However, we like to make some remarks on this based on the results shown in this paper. Two alternative views for this mechanism exist in the literature. One theory [13] is based on the extinction of non-premixed flamelets experiencing scalar dissipation rates larger than the extinction value for a given fuel. The other theory is based on the propagation of premixed flamelets [4].

Figure 20a presents the temperature field and $\widetilde{\epsilon}_{ZZ}$, normalised by a reference quenching value of 73 s^{-1} [29], near the flame stabilisation region for the Case-D. The leading edge generally experiences a low $\widetilde{\epsilon}_{ZZ}$, which is about 5% of the extinction value. This is consistent with observations in experimental [63] and numerical [29] studies. Although $\widetilde{\epsilon}_{ZZ}$ may not be the single determining factor for flame stabilisation, it is nevertheless an important factor as its effect on the mean reaction rate comes through term (II) in Eq.(18).

The premixed flame propagation theory suggests that flame stabilises at a location where the laminar flame speed for local thermo-chemical condition is balanced by the velocity of the on-coming flow [4]. Mechanisms involving triple or edge flame propagation in partial premixed combustion have also been explored in the past [2]. Figure 20b shows the fluid velocity contours along with temperature field and $\widetilde{Z} = Z_{\rm st}$ contour for the Case-D near the flame stabilisation region. As one can see in this figure, the fluid velocity at the flame leading edge is about 5 m/s, which is of the same order as the laminar flame speed of stoichiometric hydrogen-air mixture having a reactant temperature equal to the local fluid temperature. This is consistent with an experimental observation in [76]. The results in Fig. 20 seem to support the flame propagation theory, but it emphasises that the flame displacement speed, as one can easily obtain from Eq. (18), is affected by $\widetilde{\epsilon}_{ZZ}$ as seen in Eq. (18). Thus, the propagation of premixed flamelet, effects of $\widetilde{\epsilon}_{ZZ}$ and their mutual interactions influence the flame stabilisation at the leading edge in an average sense as noted earlier in Fig. 16. Much more detailed examination is required to address this issue on an instantaneous basis, which is beyond the scope of this study, and this will be addressed in future.

5. Conclusion

This paper focus on the modelling of turbulent lifted jet flames using flamelets and a presumed joint PDF approach. Both premixed and non-premixed contributions are included when calculating the mean reaction rate. The premixed part is obtained using unstrained premixed flamelets and the non-premixed part is estimated using a simple model in Eq. (19). Also, the mixture fraction, Z, and progress variable, c, are not assumed to be statistically independent and their correlation is included in the joint PDF, $P(\xi, \zeta)$, using a *copula*. *A posteriori* validation is also conducted using RANS methodology.

In the first part of this study, *a priori* assessment of various presumed PDF/flamelets models are conducted using a DNS database of a turbulent lifted hydrogen jet flame. The presumed PDFs required to calculate the mean reaction rate are tested using the DNS data. The Beta function PDF is a good approximation for the marginal PDFs of Z and c. The *copula* method [40] to get the correlated joint PDF is tested using the DNS data. This method combines the two marginal PDFs of Z and c according to a prescribed covariance, $\widetilde{Z''c''}$, see Eq. (14). The joint PDFs obtained by this method agree well with the PDFs from the DNS data.

Four flamelets/PDF models for the mean reaction rate are assessed. The unstrained premixed flamelet with a joint PDF assuming statistical independence of Z and c, **M1**, overestimates the mean reaction rate at downstream positions. However, the values given by this model at the flame base are reasonable compared to the DNS values. When the statistical correlation of Z and c is included, as for the model **M2**, the estimates of mean reaction rates are improved in general. The non-premixed flamelets model, **M3**, substantially underestimates the mean reaction rate for all axial locations, but its agreement with DNS values is reasonable for regions with diffusion controlled combustion. The recently proposed strained premixed flamelets model [42, 43], called as **M4** in this study, generally underestimates the mean reaction rate when it is extended to partially premixed combustion. The contributions to the mean reaction rate arising through three scalar dissipation rate, see Eq. (3), are also studied. The contribution from $\rho N_{cc}\left(\partial^2 Y_{\mathrm{H_2O}}/\partial c^2\right)$ becomes zero since c is linearly related to $Y_{\mathrm{H_2O}}$ in this study. The contribution from the cross dissipation related term, term (III) in Eq. (18), is very much smaller than the contribution from the term (II) as discussed in section 3.5. A simple model for term (II), signifying the contributions from non-premixed mode in partially premixed combustion, is proposed and tested using the DNS data and the agreement is satisfactory.

In the second part of this study, *a posteriori* validation of the reaction rate closures, specifically **M1** and **M2**, is conducted. The prime aim is to capture both the lift-off height and flame brush structure. It is observed that the standard unstrained premixed flamelets model with the assumption of statistical independence of Z and c, model **M1**, overestimates the mean reaction rate and yields a smaller lift-off height of about $4.5D$ compared to the experimental [47, 48] value of $7D$. The flame lift-off height increased to $5.2D$ when the contributions of the diffusion combustion are included through the term (II). The premixed flamelets model **M2** which includes the Z-c correlation gives a lift-off height of $6D$ if the term (II) is excluded. The lift-off height becomes $7.5D$ when the term (II) is included for the model **M2**. These trends clearly suggest that the effects of both Z-c correlation and non-premixed combustion are important to capture the right physics of stabilisation mechanisms at the flame base. It seems that the flame stabilisation is influenced by both premixed and non-premixed combustion modes, and their mutual influences. The flame brush structure is also captured reasonably well by the model used in this study. The flame lift-off height as function of jet velocity calculated using the **M2** model with term (II) agrees reasonably well with measured heights when the inlet turbulence level is selected carefully. This suggests that accurate flow fields are required to get correct lift-off heights. To achieve this in RANS, it is imperative that the inflow statistics must be

characterised fully by experiments otherwise, simulation approaches such as LES having the ability to capture the evolution of large scale turbulence structures and their dynamics from an arbitrary initial state may be required.

Acknowledgment

A part of this work involving DNS data analysis was performed under the collaborative program on turbulent combustion modelling between Cambridge University and JAXA. The financial support from Mitsubishi Heavy Industries, Ltd, Takasago, Japan, is gratefully acknowledged.

References

[1] W.M. Pitts, *Assessment of theories for the behavior and blowout of lifted turbulent jet diffusion flames*, Proc. Combust. Inst. 22 (1988), pp. 809–816.
[2] K.M. Lyons, *Toward an understanding of the stabilization mechanisms of lifted turbulent jet flames: Experiments*, Prog. Energy Combust. Sci. 33 (2007), pp. 211–231.
[3] C. Lawn, *Lifted flames on fuel jets in co-flowing air*, Prog. Energy Combust. Sci. 35 (2009), pp. 1–30.
[4] L. Vanquickenborne and A. van Tiggenlen, *The stabilisation mechanism of lifted diffusion flames*, Combust. Sci. Technol. 10 (1966), pp. 59–69.
[5] J.E. Broadwell, W.J.A. Dahm, and M.G. Mungal, *Blowout of turbulent diffusion flames*, Proc. Combust. Inst. 20 (1984), pp. 303–310.
[6] R.C. Miake-Lye and J.A. Hammer, *Lifted turbulent jet flames: a stability criterion based on the jet large-scale structure*, Proc. Combust. Inst. 22 (1989), pp. 817–824.
[7] C. Yoo, R. Sankaran, and J. Chen, *Three-dimensional Direct Numerical Simulation of a turbulent lifted hydrogen jet flame in heated coflow: flame stabilization and structure*, J. Fluid Mech. 640 (2009), pp. 453–481.
[8] V. Favier and L. Vervisch, *Investigating the Effects of Edge Flames in Liftoff in Non-Premixed Turbulent Combustion*, Proc. Combust. Inst. 27 (1998), pp. 1239–1245.
[9] K.A. Watson, K.M. Lyons, J.M. Donbar, and C.D. Carter, *Observations on the leading edge in lifted flame stabilization*, Combust. Flame 119 (1999), pp. 199–202.
[10] Y. Mizobuchi, S. Tachibana, J. Shinio, S. Ogawa, and T. Takeno, *A numerical analysis of the structure of a turbulent hydrogen jet lifted flame*, Proc. Combust. Inst. 29 (2002), pp. 2009–2015.
[11] A. Upatnieks, J. Driscoll, C. Rasmussen, and S. Ceccio, *Liftoff of turbulent jet flames-assessment of edge flame and other concepts using cinema-PIV*, Combust. Flame 138 (2004), pp. 252–272.
[12] L.K. Su, O.S. Sun, and M.G. Mungal, *Experimental investigation of stabilization mechanisms in turbulent, lifted jet diffusion flames*, Combust. Flame 144 (2006), pp. 494–512.
[13] N. Peters and F.A. Williams, *Liftoff characteristics of turbulent jet diffusion flames*, AIAA J. 21 (1983), pp. 423–429.
[14] P. Domingo, L. Vervisch, and J. Réveillon, *DNS analysis of partially premixed combustion in spray and gaseous turbulent flame-bases stabilized in hot air*, Combust. Flame 140 (2005), pp. 172–195.
[15] P. Domingo, L. Vervisch, and D. Veynante, *Large Eddy Simulation of a lifted methane jet flame in a vitiated coflow*, Combust. Flame 152 (2008), pp. 415–432.
[16] C.S. Yoo, E.S. Richardson, R. Sankaran, and J.H. Chen, *A DNS study on the stabilization mechanism of a turbulent lifted ethylene jet flame in highly-heated coflow*, Proc. Combust. Inst. 33 (2011), pp. 1619–1627.
[17] C.M. Müller, H. Breitbach, and N. Peters, *Partially premixed turbulent flame propagation in jet flames*, Proc. Combust. Inst. 25 (1994), pp. 1099–1106.
[18] M. Chen, M. Herrmann, and N. Peters, *Flamelet Modeling of Lifted Turbulent Methane/Air and Propane/Air Jet Diffusion Flames*, Proc. Combust. Inst. 28 (2000), pp. 167–174.
[19] N. Peters, *Turbulent Combustion* Cambridge University Press, 2000.
[20] D. Bradley, P.H. Gaskell, and A.K.C. Lau, *A Mixedness-Reactedness Flamelet Model for Turbulent Diffusion Flames*, Proc. Combust. Inst. 23 (1990), pp. 685–692.
[21] D. Bradley, P.H. Gaskell, and X.J. Gu, *The Mathematical Modelling of Liftoff and Blowoff Turbulent Non-premixed Methane Jet Flames at High Strain Rates*, Proc. Combust. Inst. 27 (1998), pp. 1199–1206.
[22] P. Domingo, L. Vervisch, and K.N.C. Bray, *Partially premixed flamelets in LES of non-premixed turbulent combustion*, Combust. Theory Model. 6 (2002), pp. 529–551.
[23] C. Ma, T. Mahmuda, M. Fairweather, E. Hampartsoumian, and P. Gaskell, *Prediction of lifted, non-premixed turbulent flames using a mixedness-reactedness flamelet model with radiation heat loss*, Combust. Flame 128 (2002), pp. 60–73.
[24] L. Vervisch, R. Hauguel, P. Domingo, and M. Rullaud, *Three facets of turbulent combustion modelling: DNS of premixed V-flame, LES of lifted nonpremixed flame and RANS of jet-flame*, J. Turbulence 5 (2004), p. 004.
[25] S.A. Ferraris and J.X. Wen, *Large Eddy Simulation of a lifted turbulent jet flame*, Combust. Flame 150 (2007), pp. 320–339.
[26] A.W. Vreman, B.A. Albrecht, J.A. van Oijen, L.P.H. de Goey, and R.J.M. Bastiaans, *Premixed and nonpremixed generated manifolds in Large Eddy Simulation of Sandia flame D and F*, Combust. Flame 153 (2008), pp. 394–416.
[27] J.B. Michel, O. Colin, C. Angelberger, and D. Veynante, *Using the tabulated diffusion flamelet model ADF-PCM to simulate a lifted methane-air jet flame*, Combust. Flame 156 (2009), pp. 1318–1331.
[28] C. Devaud and K.N.C.. Bray, *Assessment of the applicability of Conditional Moment Closure to a lifted turbulent flame: first order model*, Combust. Flame 132 (2003), pp. 102–114.
[29] I. Kim and E. Mastorakos, *Simulations of turbulent lifted jet flames with two-dimensional conditional moment closure*, Proc. Combust. Inst. 30 (2005), pp. 911–918.

[30] S. Navarro-Martinez and A. Kronenburg, *Flame Stabilization Mechanisms in Lifted Flames*, Flow Turbulence Combust. 87 (2011), pp. 377–406.
[31] R.R. Cao, S.B. Pope, and A.R. Masri, *Turbulent lifted flames in a vitiated coflow investigated using joint PDF calculations*, Combust. Flame 142 (2005), pp. 438–453.
[32] J.A. van Oijen and L.P.H. de Goey, *Modelling of Premixed Laminar Flames using Flamelet-Generated Manifolds*, Combust. Sci. Technol. 161 (2000), pp. 113–137.
[33] O. Gicquel, N. Darabiha, and D. Thévenin, *Laminar Premixed Hydrogen/Air counterflow flame simulation using Flame Prolongation of ILDM with Differential Diffusion*, Proc. Combust. Inst. 28 (2000), pp. 1901–1908.
[34] H. Yamashita, M. Shimada, and T. Takeno, *A numerical study on flame stability at the transition point of jet diffusion flames*, Proc. Combust. Inst. 26 (1996), pp. 27–34.
[35] E. Knudsen and H. Pitsch, *A general flamelet transformation useful for distinguishing between premixed and non-premixed modes of combustion*, Combust. Flame 156 (2009), pp. 678–696.
[36] D. Bradley, P.H. Gaskell, and X.J. Gu, *Application of a Reynolds Stress, Stretched Flamelet, Mathematical Model to Computations of Turbulent Burning Velocities and Comparison with Experiments*, Combust. Flame 96 (1996), pp. 221–248.
[37] S. Ruan, N. Swaminathan, K.N.C. Bray, Y. Mizobuchi, and T. Takeno, *Scalar and its dissipation in the near field of turbulent lifted jet flame*, Combust. Flame 159 (2012), pp. 591–608.
[38] Y. Mizobuchi, J. Shinjo, S. Ogawa, and T. Takeno, *A numerical study on the formation of diffusion flame islands in a turbulent hydrogen jet lifted flame*, Proc. Combust. Inst. 30 (2005), pp. 611–619.
[39] O. Darbyshire, *Modelling of Turbulent Stratified Flames*, University of Cambridge, 2011.
[40] O. Darbyshire and N. Swaminathan, *A Presumed Joint PDF Model for Turbulent Combustion with Varying Equivalence Ratio*, Combust. Sci. Technol. 184 (2012), pp. 2036–2067.
[41] E.R. Hawkes and J.H. Chen, *Comparison of direct numerical simulation of lean premixed methane-Air flames with strained laminar flame calculations*, Combust. Flame 144 (2006), pp. 112–125.
[42] H. Kolla and N. Swaminathan, *Strained flamelets for turbulent premixed flames, I: Formulation and planar flame results*, Combust. Flame 157 (2010), pp. 943–954.
[43] H. Kolla and N. Swaminathan, *Strained flamelets for turbulent premixed flames II: Laboratory flame results*, Combust. Flame 157 (2010), pp. 1274–1289.
[44] K.N.C. Bray, P. Domingo, and L. Vervisch, *Role of the progress variable in models for partially premixed turbulent combustion*, Combust. Flame 141 (2005), pp. 431–437.
[45] R.W. Bilger, *The structure of diffusion flames.*, Combust. Sci. Technol. 13 (1976), pp. 155–170.
[46] N. Peters, *Laminar Diffusion Flamelet Models in Non-premixed Turbulent Combustion*, Prog. Energy Combust. Sci. 10 (1984), pp. 319–339.
[47] T. Cheng, J.A. Wehrmeyer, and R.W. Pitz, *Simultaneous Temperature and Multispecies Measurement in a Lifted Hydrogen Diffusion Flame*, Combust. Flame 91 (1992), pp. 323–345.
[48] T. Cheng, J. Wehrmeyer, and R. Pitz, *Conditional analysis of lifted hydrogen jet diffusion flame experimental data and comparison to laminar flame solutions*, Combust. Flame 150 (2007), pp. 340–354.
[49] C.K. Westbrook, *Hydrogen Oxidation Kinetics in Gaseous Detonations*, Combust. Sci. Technol. 29 (1982), pp. 67–82.
[50] R.W. Bilger, *Turbulent Flows with Nonpremixed Reactants*, in *Turbulent Reacting Flows*, P.A. Libby and F.A. Williams, eds., Springer-Verlag, 1980.
[51] K. Bray, M. Champion, P. Libby, and N. Swaminathan, *Finite rate chemistry and presumed PDF models for premixed turbulent combustion*, Combust. Flame 146 (2006), pp. 665–673.
[52] R.L. Plackett, *A class of bivariate distributions*, J. Am. Stat. Assoc. 60 (1965), pp. 516–522.
[53] E. Effelsberg and N. Peters, *Scalar dissipation rates in turbulent jets and jet diffusion flames*, Proc. Combust. Inst. 22 (1988), pp. 693–700.
[54] V. Eswaran and S.B. Pope, *Direct Numerical Simulation of the turbulent mixing of a passive scalar*, Phys. Fluids 31 (1988), pp. 506–520.
[55] F. Gao and E.O. Brien, *Joint probability density function of a scalar and its gradient in isotropic turbulence*, Phys. Fluids A 3 (1991), pp. 1625–1632.
[56] S. Bondi and W.P. Jones, *A combustion model for premixed flames with varying stoichiometry*, Proc. Combust. Inst. 29 (2002), pp. 2123–2129.
[57] T. Landenfeld, A. Sadiki, and J. Janicka, *A turbulence-chemistry interaction model based on a multivariate presumed beta-pdf method for turbulent flames*, Flow Turb. Combust. 68 (2002), pp. 111–135.
[58] E. Schneider, A. Maltsev, A. Sadiki, and J. Janicka, *Study on the potential of BML-approach and G-equation concept-based models for predicting swirling partially premixed combustion systems: URANS computations*, Combust. Flame 152 (2008), pp. 548–572.
[59] S.P. Malkeson and N. Chakraborty, *Statistical Analysis of Cross Scalar Dissipation Rate Transport in Turbulent Partially Premixed Flames: A Direct Numerical Simulation Study*, Flow Turbulence Combust. 87 (2011), pp. 313–349.
[60] W.P. Jones and B.E. Launder, *The prediction of laminarization with a two equation model of turbulence*, Int. J. Heat Mass Transfer. 15 (1972), pp. 301–314.
[61] W.P. Jones, *Turbulence modelling and numerical solution methods for variable density and combusting flows*, in *Turbulent Reacting Flows*, P.A. Libby and F.A. Williams, eds., Academic Press, New York, 1994.
[62] S. Zhang and C.J. Rutland, *Premixed Flame Effects on Turbulence and Pressure-Related Terms*, Combust. Flame 102 (1995), pp. 447–461.
[63] A. Brockhinke, S. Haufe, and K. Kohse-Höinghaus, *Structural Properties of Lifted Hydrogen Jet Flames Measured by Laser Spectroscopic Techniques*, Combust. Flame 121 (2000), pp. 367–377.
[64] K.N.C. Bray and P.A. Libby, *Recent developments in the BML model of premixed turbulent combustion*, in *Turbulent Reacting Flows*, P.A. Libby and F.A. Williams, eds., Academic Press, New York, 1994, pp. 115–151.
[65] N. Swaminathan and K.N.C. Bray, *Fundamentals and challenges*, in *Turbulent Premixed Flames*, N. Swaminathan and K.N.C. Bray, eds., Cambridge University Press, 2011.
[66] D.B. Spalding, *Concentration fluctuations in a round turbulent free jet*, Chem. Eng. Sci. 26 (1971), pp. 95–107.
[67] T. Mantel and R.W. Bilger, *Some Conditional Statistics in a Turbulent Premixed Flame Derived from Direct Numerical Simulation*, Combust. Sci. Technol. 110-111 (1995), pp. 393–417.
[68] N. Swaminathan and K.N.C. Bray, *Effect of dilatation on scalar dissipation in turbulent premixed flames*, Combust.

Flame 143 (2005), pp. 549–565.
[69] H. Kolla, J.W. Rogerson, N. Chakraborty, and N. Swaminathan, *Scalar Dissipation Rate Modeling and its Validation*, Combust. Sci. Technol. 181 (2009), pp. 518–535.
[70] O.R. Darbyshire, N. Swaminathan, and S. Hochgreb, *The Effects Of Small-Scale Mixing Models On The Prediction Of Turbulent Premixed And Stratified Combustion*, Combust. Sci. Technol. 182 (2010), pp. 1141–1170.
[71] N. Chakraborty, J.W. Rogerson, and N. Swaminathan, *A priori assessment of closures for scalar dissipation rate transport in turbulent premixed flames using Direct Numerical Simulation*, Phys. Fluids 20 (2008), p. 045106.
[72] J.W. Rogerson and N. Swaminathan, *Correlation between dilatation and scalar dissipation in turbulent premixed flames*, Proc. European Combustion Meeting 2007 (2007).
[73] D.B. Spalding, *Combustion and Mass Transfer* Oxford University Press, 1979.
[74] I. Glassman, *Combustion* 2nd ed., Academic Press Inc, 1987.
[75] S. Ruan, *Turbulent Partially Premixed Combustion: DNS Analysis and RANS Simulation*, University of Cambridge, 2012.
[76] L. Muniz and M.G. Mungal, *Instantaneous flame-stabilization velocities in lifted-jet diffusionFlames*, Combust. Flame 111 (1997), pp. 16–31.

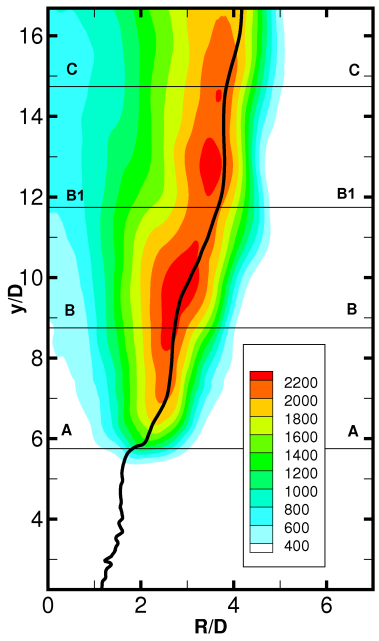

Figure 1. The averaged temperature field and stoichiometric mixture fraction contour from the DNS data. The nozzle exit is located at $y/D = 0$.

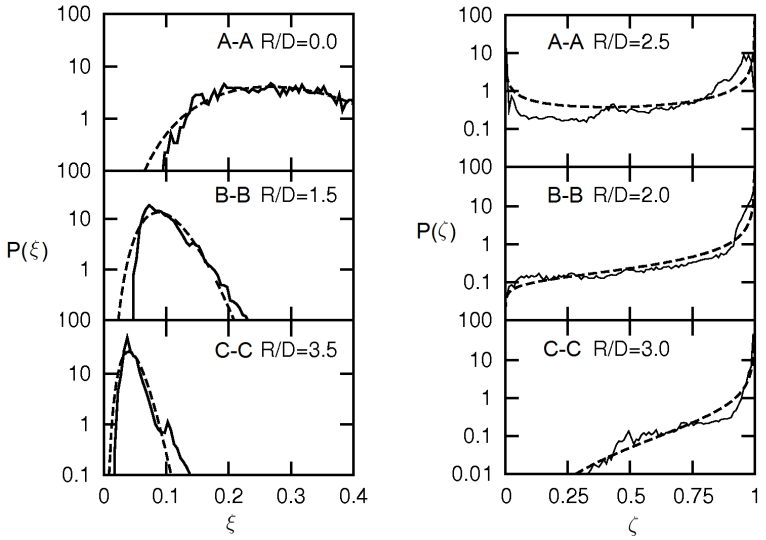

Figure 2. Comparison of mixture fraction and progress variable PDFs from the DNS (solid line) and β function model (dashed) at different axial and radial positions. The axial positions are marked in Fig. 1

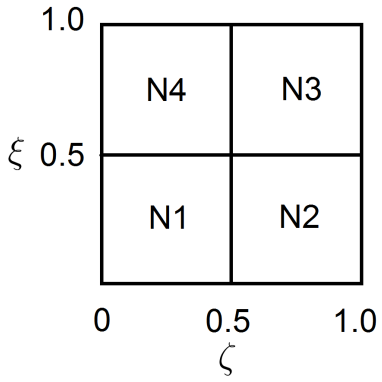

Figure 3. Contingency table. N_i is the number of samples falling in each quadrant.

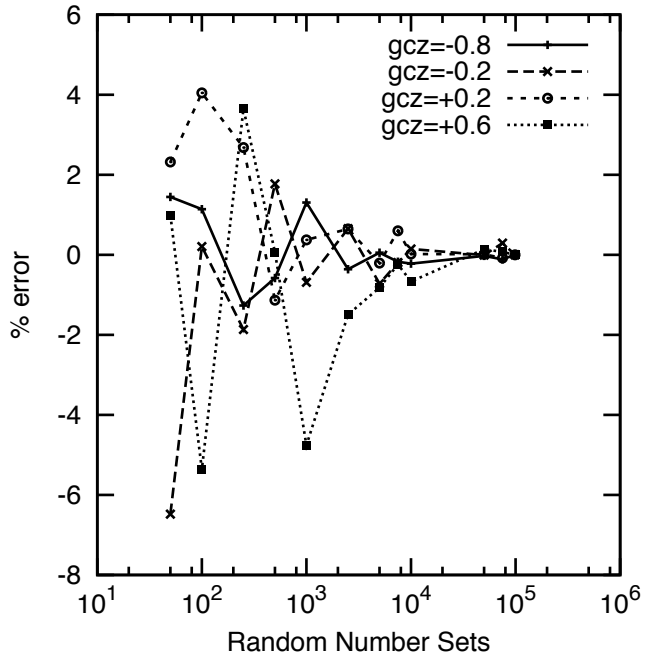

Figure 4. Errors in mean reaction rate for $\widetilde{Z} = 0.03$, $\widetilde{c} = 0.7$, $\widetilde{Z''^2} = 0.000291$ and $\widetilde{c''^2} = 0.105$ against the number of random sample sets used in computing the joint PDF.

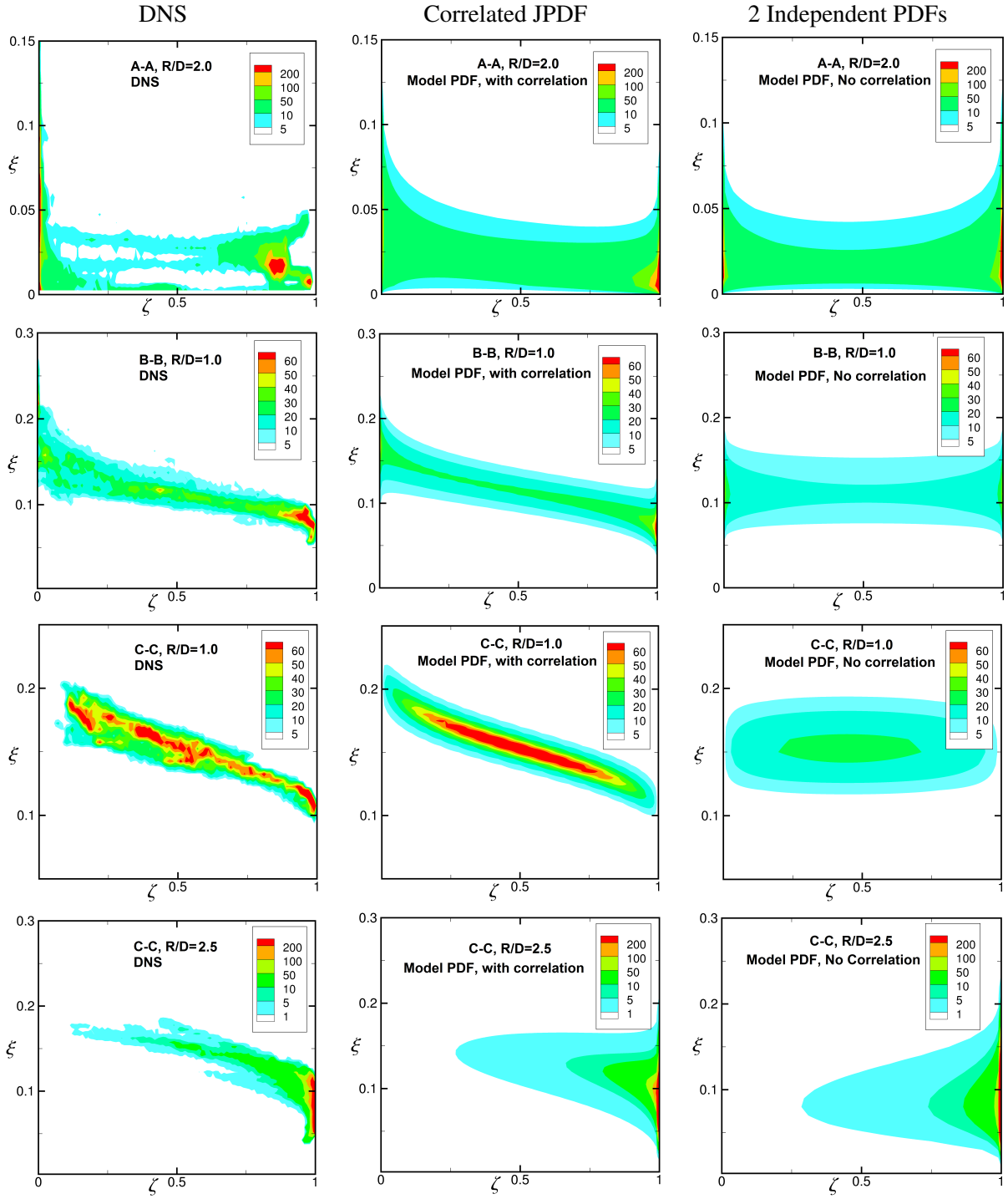

Figure 5. Comparison of joint PDF, $P(\xi, \zeta)$, obtained from the DNS data (left column) and modelled PDF with correlation (middle) and without correlation (right). The first part of Eq. (14) gives the correlated PDF and its second part gives the independent PDF. First row: position A-A and $R/D = 2.0$, second row: B-B and $R/D = 1.0$, third row: C-C and $R/D = 1.0$, and fourth row: C-C, $R/D = 2.5$.

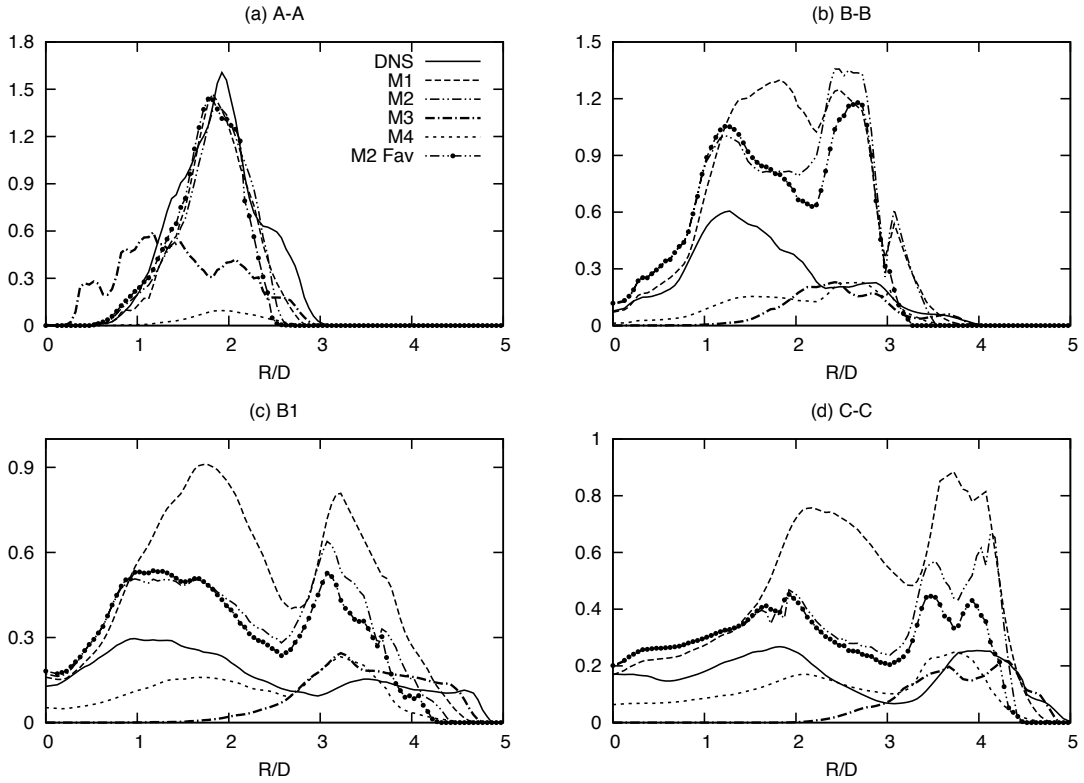

Figure 6. Comparison of DNS and modelled mean reaction rates $\overline{\dot{\omega}_c}$ (g/cm^3/s) at positions (a) A-A, (b) B-B, (c) B1 and (d) C-C illustrated in Fig.1.

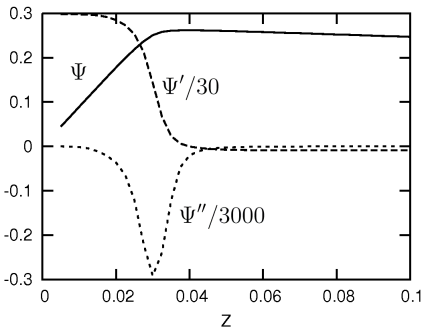

Figure 7. Variation of $\Psi = Y_{H2O}^{Eq}$, $d\Psi/dZ$ and $d^2\Psi/dZ^2$ with the mixture fraction, Z.

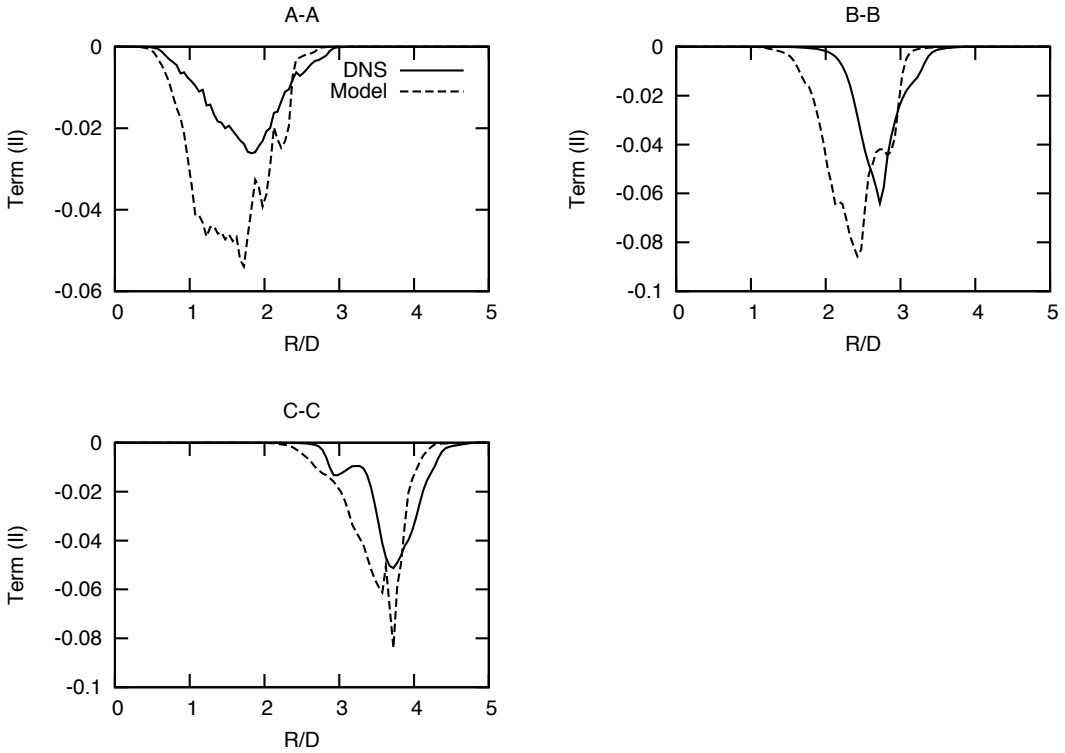

Figure 8. Comparison of term (II) DNS results and model in Eq. (19) at different axial positions.

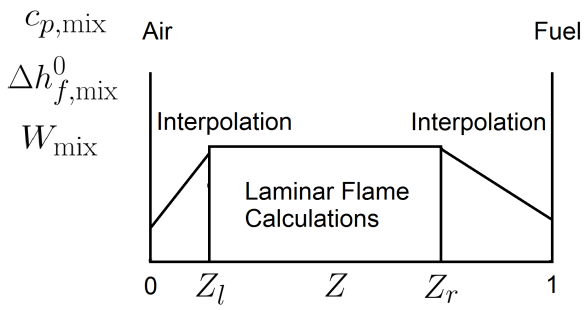

Figure 9. Illustration of mixture properties such as $c_{p,\mathrm{mix}}$, $\Delta h^0_{f,\mathrm{mix}}$ and W_{mix} calculation.

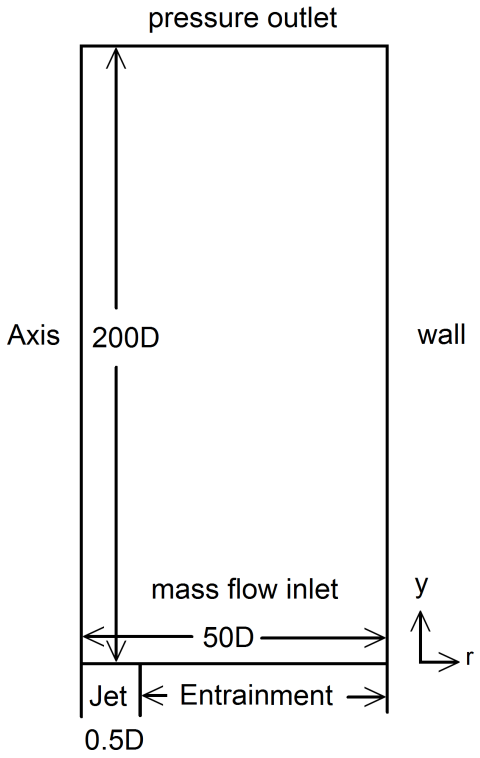

Figure 10. Schematic of the computational domain for RANS simulations of this study.

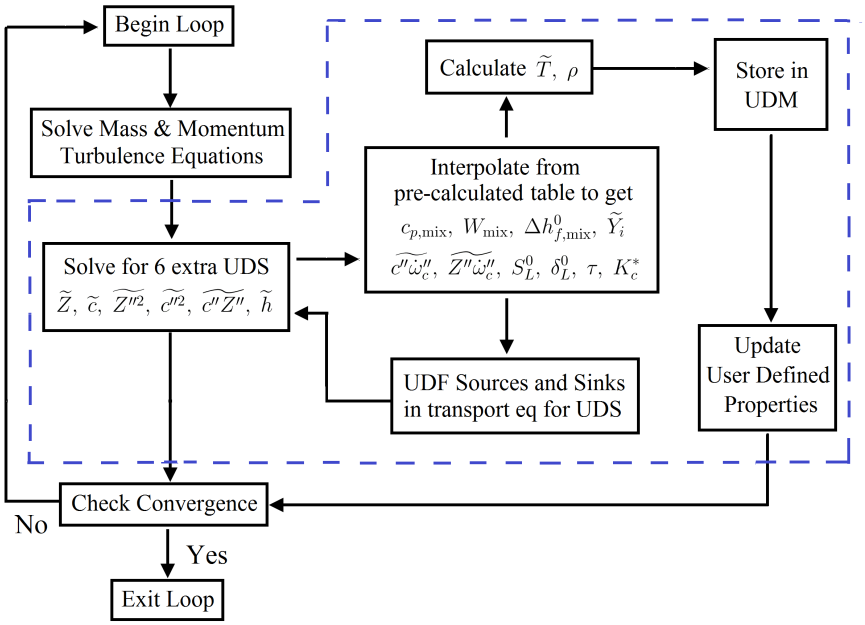

Figure 11. Flow chart for calculation steps involved in RANS simulations of this study. The part within the dashed line is developed in this study.

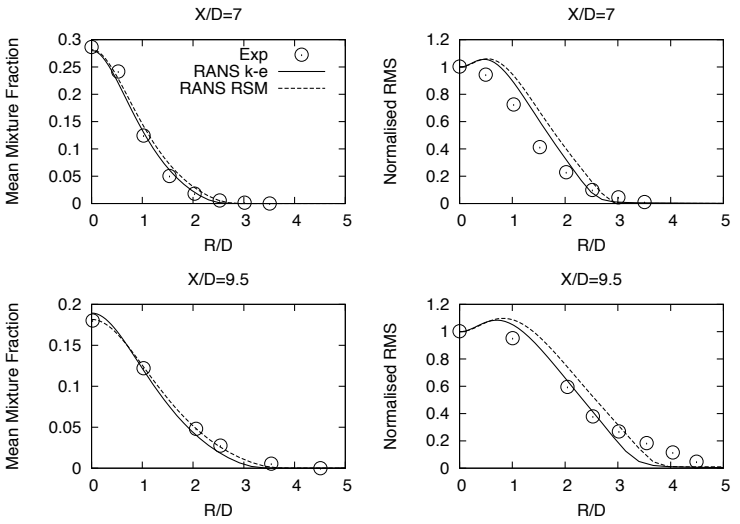

Figure 12. Comparison of simulation results with experimental measurements [47] of the mean mixture fraction and RMS values normalised by the respective centreline values. The results are shown for $y = 7D$ and $9.5D$.

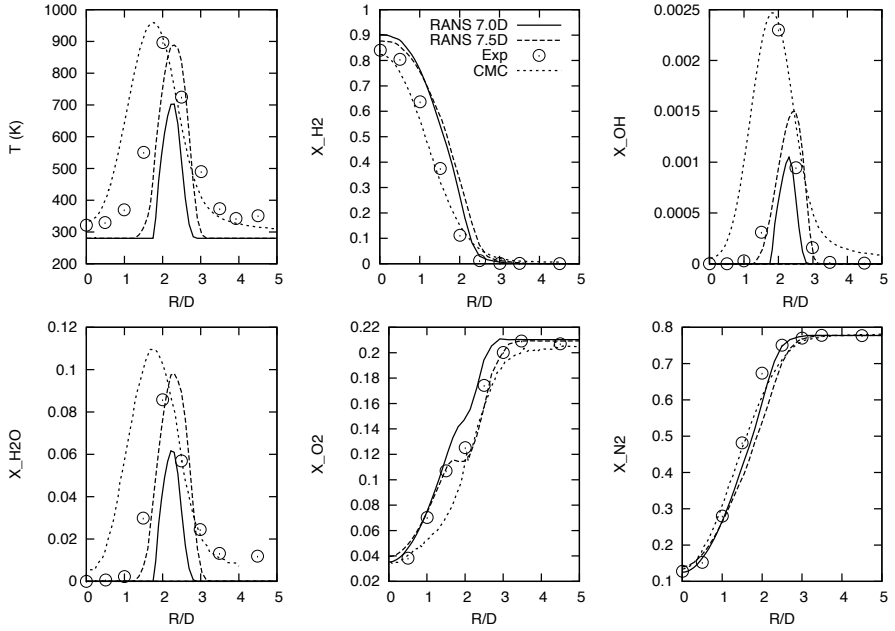

Figure 13. Comparison of simulation results (7D and 7.5D), experimental measurements [47] and CMC results [28] for radial variation of scalar values.

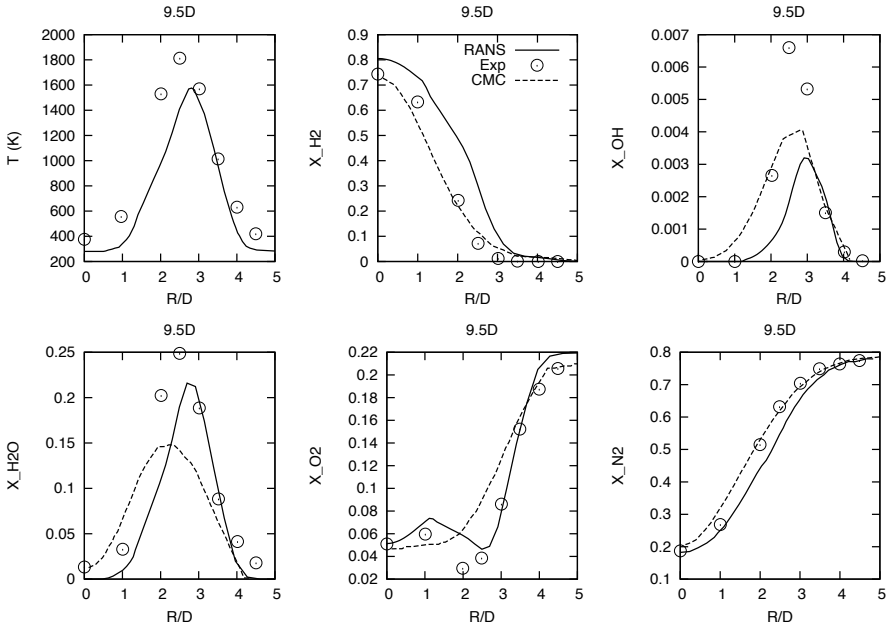

Figure 14. Comparison of simulation results, experimental measurements [47] and CMC results [29] for radial variation of scalar values at $y = 9.5D$. The CMC result for temperature is unavailable.

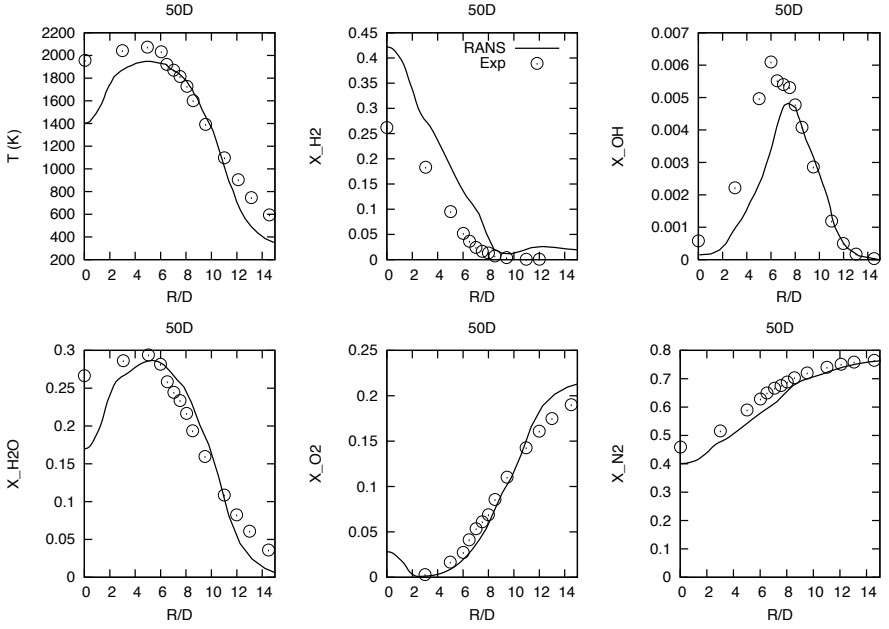

Figure 15. Comparison of simulation results and experimental measurements [47] of radial variation of scalar values at $y = 50D$.

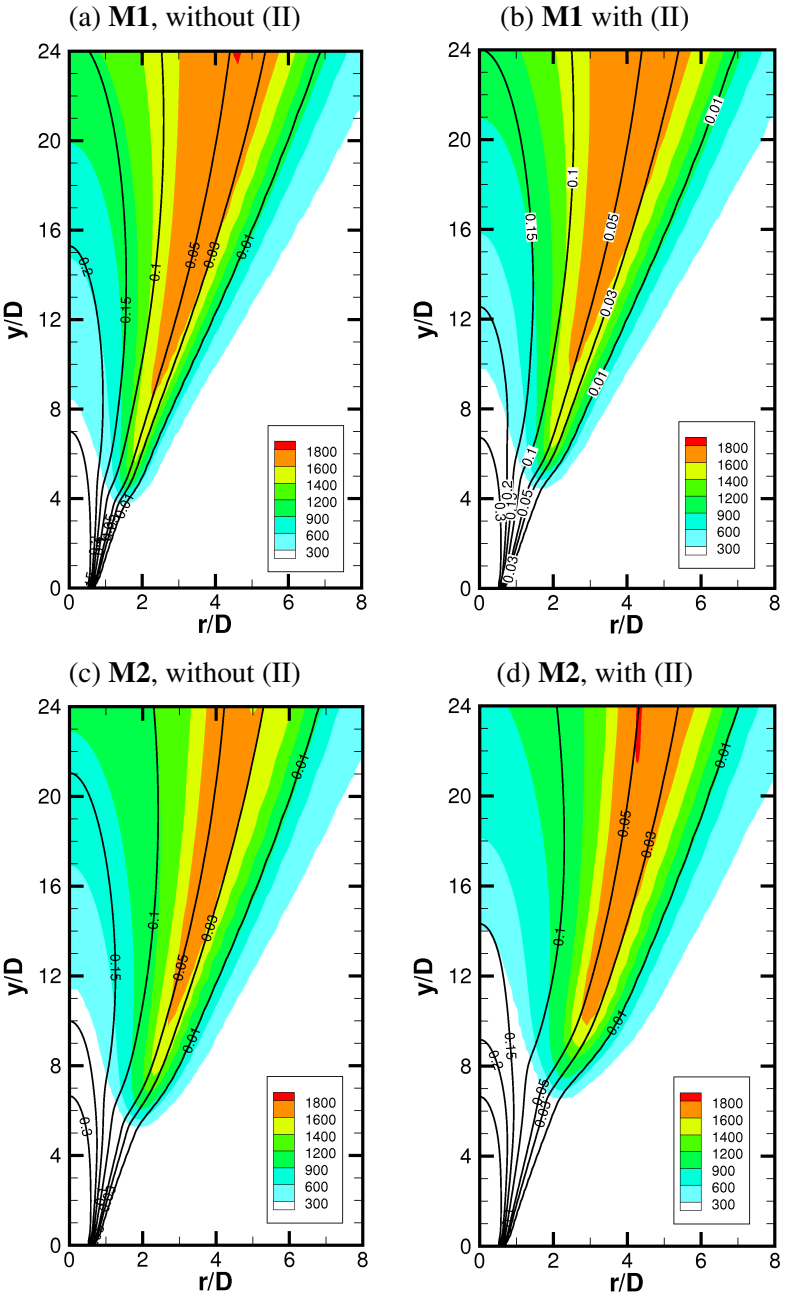

Figure 16. Comparison of flame lift-off heights for four cases in Table 2; (a) Case-A, (b) Case-B, (c) Case-C, (d) Case-D. The contour lines are $\widetilde{Z}$.

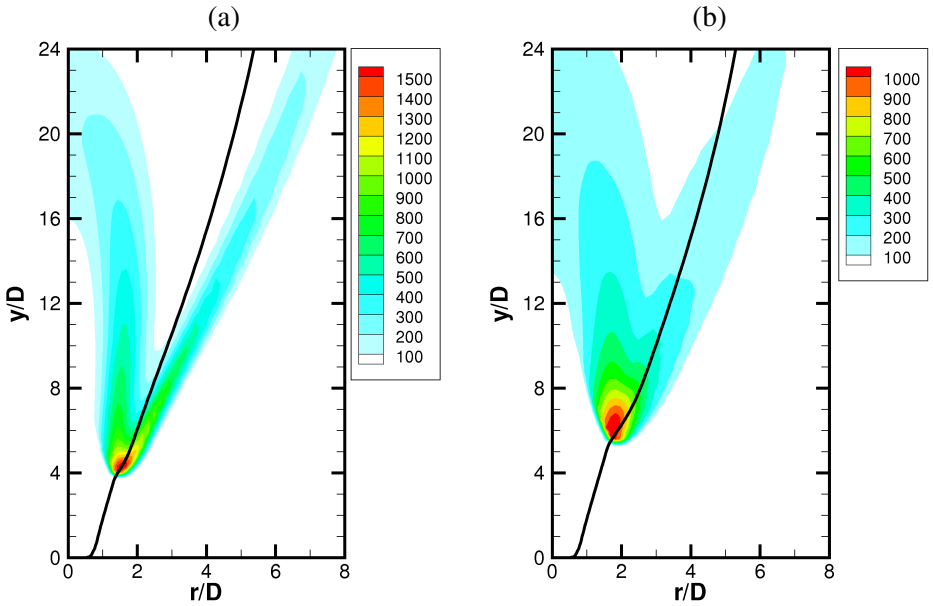

Figure 17. Effect Z-c correlation on the mean reaction rate (kg/m^3/s); (a) Case-A and (b) Case-C.

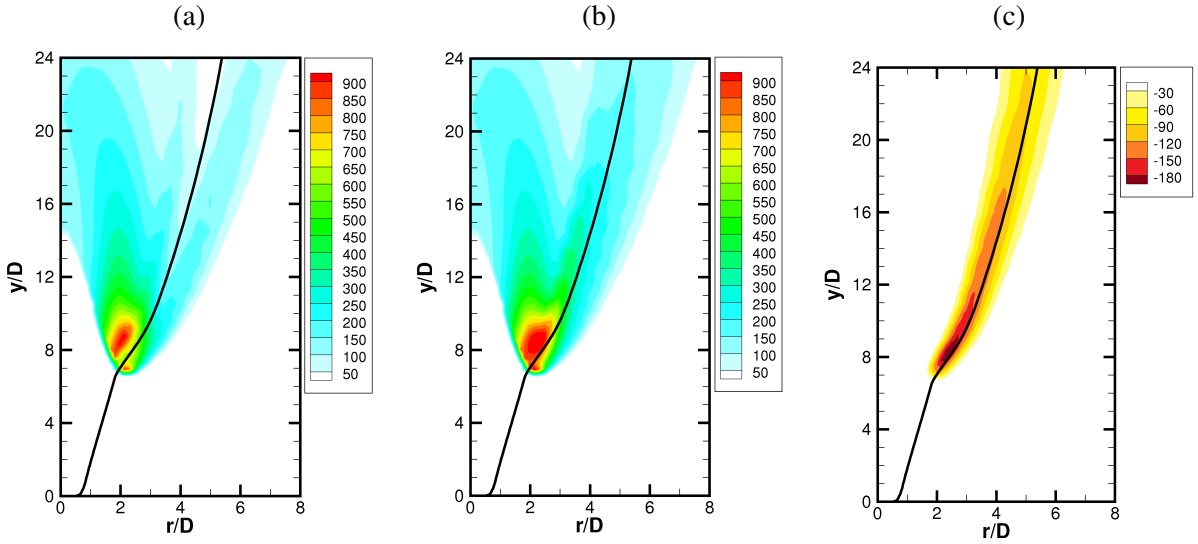

Figure 18. Mean reaction rate (kg/m^3/s) for Case-D. (a) Total reaction rate $\overline{\dot{\omega}}_c^*$ in Eq. (18); (b) Term (I), $\overline{\dot{\omega}}_c$, in Eq. (18); (c) Term (II) as in Eq.(19).

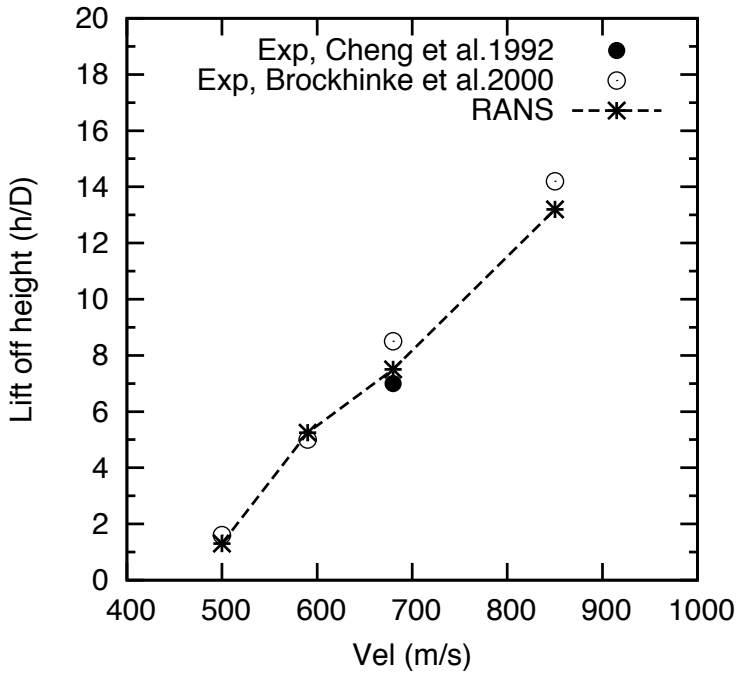

Figure 19. Flame lift-off height versus jet velocity.

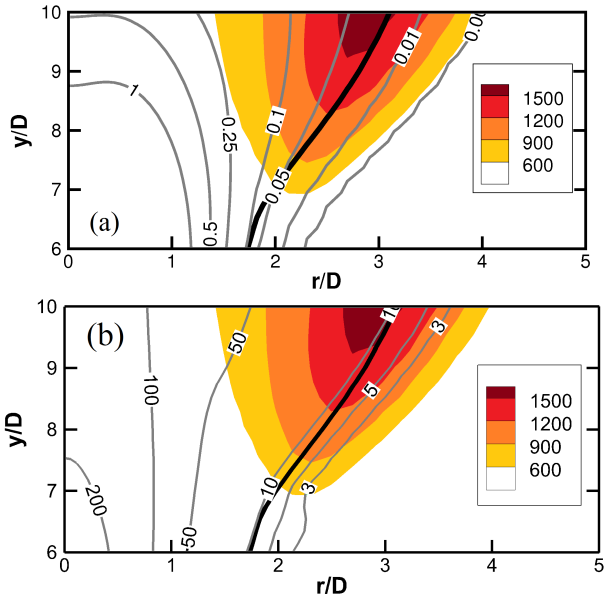

Figure 20. Temperature field with (a) $\widetilde{\epsilon}_{ZZ}$ and (b) fluid velocity in m s^{-1} (thin lines) near the flame stabilisation region for Case-D in Table 2. Values of $\widetilde{\epsilon}_{ZZ}$ are normalised using the extinction value of 73 s^{-1} for laminar diffusion flame. Stoichiometric mixture fraction contour is also shown using a thick line.